

# Critical Behavior of Charge Density Waves

## Below Threshold: Numerical and Scaling Analysis

Daniel S. Fisher

*Lyman Laboratories, Harvard University, Cambridge MA 02138*

A. Alan Middleton

*Physics Department, Syracuse University, Syracuse, NY 13244*

(Received )

The critical behavior of pinned charge density waves (CDW's) is studied as the threshold for sliding is approached. Using the Fukuyama-Lee-Rice Hamiltonian with relaxational dynamics, the polarization and linear response are calculated numerically. Analytic bounds on the subthreshold motion are used to develop fast numerical algorithms for evolving the CDW configuration. Two approaches to threshold, "reversible" and "irreversible" are studied, which differ in the details of the critical behavior. On the irreversible approach to threshold, the response due to avalanches triggered by local instabilities dominates the polarizability, which diverges in one and two dimensions. Such "jumps" are absent on the reversible approach. On both the reversible and irreversible approach in two dimensions, the linear response, which does not include the jumps, is singular, but does not diverge. Characteristic diverging length scales are studied using finite-size scaling of the sample-to-sample variations of the threshold field in finite systems and finite-size effects in the linear polarizability and the irreversible polarization. A dominant diverging correlation length is found which controls the threshold field distribution, finite-size effects in the irreversible polarization, and a cutoff size for the avalanche size distribution. This length diverges with an exponent  $\nu \approx 2.0, 1.0$  in dimensions  $d = 1, 2$ , respectively. A

distinct exponent describes the finite-size effects for the linear polarizability in single samples. Our results are compared with those for related models and questions are raised concerning the relationship of the static critical behavior below threshold to the dynamic critical behavior in the sliding state above threshold.

## I. INTRODUCTION

Despite many years of experimental and theoretical work [1], much of the behavior of systems which exhibit sliding charge density waves (CDW's) is still puzzling. For most collective properties of these materials, both thermal fluctuations and defects in the charge density waves (e.g., dislocations) appear to play minor roles. The main problem is thus that of an elastic medium moving through a random potential caused by impurities. Such systems are quite ubiquitous [2], arising for weakly pinned vortex lattices in superconductors and various kinds of driven interfaces in inhomogeneous media.

The phenomenology of the CDW is based on the existence of two “phases”. Above a sharp threshold driving force,  $F_T$ , proportional to the electric field, the CDW moves with a non-zero mean velocity  $v$ , and the behavior appears to be history independent. One of us has proved elsewhere that in this regime there is a unique periodic steady state [3] for CDW models without dislocations. Below the threshold force, on the other hand, the CDW relaxes towards one of many metastable minima and is then stationary at long times (neglecting slow, thermally activated creep processes [3–6]). In this regime, the behavior is strongly hysteretic due to the many minima. As threshold is approached from below, sections of the CDW become unstable and start to slide locally, only to be stopped by neighboring regions which are more strongly pinned. These give rise to a non-linear response to changes in  $F$ . The cascade of avalanches which occurs bears considerable resemblance to that found in other systems with collective transport, for example models of “sand piles” and motion of geologic faults [7,8]. The maximum size of these “avalanches” diverges as threshold is approached, leading eventually to the sliding of the whole system. It is the properties of CDW's as threshold is approached from below that will be the main subject of this paper.

## A. Model

The model of CDW's that we study is a simplified version of the Fukuyama-Lee-Rice Hamiltonian [9]. This model focuses on the phases  $\varphi_i$  of the CDW at impurity sites  $i = 1, \dots, N$ , which, for simplicity, are chosen to lie on a regular linear, square, or cubic lattice of dimension  $d$ . Each impurity favors a fixed random phase of the CDW,  $\beta_i$ , modulo  $2\pi$ , and couples to the phases with strength  $h$ , which we take to be uniform. The effective Hamiltonian is then [4,9–12]

$$\mathcal{H} = \frac{1}{2} \sum_{(i,j)} (\varphi_j - \varphi_i)^2 - h \sum_{i=1}^N \cos(\varphi_i - \beta_i) - F(t) \sum_{i=1}^N \varphi_i, \quad (1.1)$$

where the first term represents the elastic interactions between the CDW at nearest neighbor impurity sites  $(i, j)$  and the last term represents the effect of a spatially uniform driving force  $F$ , which may be a function of the time  $t$ . The equations of motion are purely relaxational [1,9,10,12,13]

$$\frac{d\varphi_i}{dt} = -\frac{\partial \mathcal{H}}{\partial \varphi_i} = \Delta \varphi_i + h \sin(\varphi_i - \beta_i) + F \quad (1.2)$$

so that the system just slides down the many dimensional potential given by Eq. (1.1). Here  $\Delta \varphi_i \equiv \sum_{\delta} (\varphi_{i+\delta} - \varphi_i)$ , with  $\delta$  the nearest neighbor vectors, is the lattice Laplacian. The preferred phases  $\{\beta_i\}$  are independent, uniformly distributed, random variables, chosen in the interval  $[0, 2\pi)$ .

Because of the non-linear nature of the equations of motion, very few analytic results are available: perturbation theory [10,14] is possible only for large fields  $F \gg F_T$  and some general bounds on the behavior can be derived (see Sec. II and Ref. [3]). Mean field theory, valid in the limit of long range elastic interactions, has been investigated by one of us in some detail [4], but expansions about mean field theory are difficult, although very recently progress has been made above threshold [15]. Since we are interested in the critical behavior near threshold in finite-dimensional systems, we have thus resorted to extensive numerical simulations, making use of analytic bounds. The numerical methods are discussed in Sec. III.

## B. Results for polarization for two approaches to threshold

For the simulations, we use periodic boundary conditions on one, two, and three dimensional “cubes” of volume  $L^d$ . Starting from an initial configuration  $\varphi_i^{\text{init}}$ , which is obtained after relaxing to a local minimum of  $\mathcal{H}$ , we adiabatically increase (or decrease) the uniform force  $F$ , letting the  $\{\varphi_i\}$  relax to a local minimum for each value of  $F$ . One of the primary quantities that we study in Sec. IV is the polarization (density)

$$P \equiv L^{-d} \sum_i (\varphi_i - \varphi_i^{\text{init}}). \quad (1.3)$$

As  $F$  is increased, the polarization increases both by continuous motion — due to the smooth evolution of the local minimum — and by discontinuous jumps which occur when the local minimum of  $\mathcal{H}$ , in which the CDW configuration is, disappears, i.e., a *local* saddle node bifurcation takes place. Except on the set of measure zero in  $F$  for which the jumps occur, we can define a linear a.c. polarizability density as the response to an infinitesimal additional a.c. force  $\delta F(\omega)$ :

$$\chi(\omega) \equiv \frac{\delta \langle \varphi(\omega) \rangle}{\delta F(\omega)} \quad (1.4)$$

where  $\langle \varphi \rangle \equiv L^{-d} \sum \varphi_i$ . In the limit of zero frequency, the linear d.c. polarizability  $\chi_0 \equiv \chi(\omega \rightarrow 0)$  will *not* in general be equal to the derivative of the polarization density, because of the discontinuous jumps. Although precursors to the jumps contribute to  $\chi_0$ , the discontinuous changes in polarization resulting from the jumps themselves are not included in  $\chi_0$ . As we will see, however, we can define a polarizability for increasing  $F$  by

$$\chi^\uparrow(F) = \lim_{\delta F \rightarrow 0^+} \lim_{L \rightarrow \infty} \frac{P(F + \delta F) - P(F)}{\delta F}, \quad (1.5)$$

which *does* include the jumps. If  $F$  is subsequently decreased, the regions that jumped forward on increasing  $F$  will, because of hysteresis [4,12], not jump back in the same fashion, so that *in general*,

$$\chi^\downarrow(F) \neq \chi^\uparrow(F) \neq \chi_0(F) \neq \chi^\downarrow(F), \quad (1.6)$$

where  $\chi^\downarrow(F)$  is defined as is in Eq. (1.5), but with the limit  $\delta F \rightarrow 0^-$ . Nevertheless, there are special system histories in which no jumps occur and for which all the polarizabilities are equal.

In order to get reproducible results which do not depend on the initial conditions, we study a particular history: increasing  $F$  initially to  $F_T^+$ , the threshold force for positive  $F$ , then decreasing the force to the opposite threshold  $F_T^- < 0$ , and then back up to  $F_T^+$ .

Since the last local minimum of  $\mathcal{H}$  to disappear as  $F$  is increased is *unique* [3] (up to uniform shifts of all phases by a multiple of  $2\pi$ ), the configuration at  $F_T^+$  (and likewise at  $F_T^-$ ) is unique. After the first increase to  $F_T^+$ , the system can be cycled back and forth to  $F_T^-$ . On the now-uniquely-defined subsequent increases to  $F_T^+$  (and generically on the initial increase), the jumps in  $P$  become larger as  $F_T^+$  is approached as larger regions of the system reach local thresholds, go unstable, and increase the elastic forces on their neighboring regions. Right at threshold, a local instability leads to motion of the whole system by  $2\pi$ . Thus we anticipate that there should be a correlation length characterizing the size of the ‘‘avalanches’’ which diverges as  $F \nearrow F_T^+$ .

Concomitantly, the polarizability  $\chi^\uparrow$  diverges, on the *irreversible approach* to threshold, with a divergence of the form

$$\chi^\uparrow(F) \sim (F_T - F)^{-\gamma}. \quad (1.7)$$

The polarization itself will also diverge if  $\gamma > 1$ . The d.c. linear polarizability,  $\chi_0$ , will be strongly dependent on  $F$  with this approach to threshold, but as shown below in Sec. IV, it will follow a curve which is *smooth* almost everywhere in the limit  $L \rightarrow \infty$  and which is distinct from  $\chi^\uparrow$ . Equivalently, one can calculate the configuration averaged  $\overline{\chi_0(F)}$ , which does not include the effects of the jumps. The precursors to jumps will not contribute significantly to this mean. As  $F \nearrow F_T^+$ , we find in the limit of an infinite system

$$\chi_0(F) \approx \chi_T - A^I (F_T^+ - F)^{-\gamma_\ell^I} \quad (1.8)$$

with the exponent  $\gamma_\ell^I < 0$ , so that  $\chi_0(F)$  exhibits only an upwards cusp to a constant value  $\chi_T$  at threshold. (Note that in any finite system  $\chi_0(F)$  diverges as  $(F_T^+ - F)^{-1/2}$ ; but the

amplitude of this divergence is negligible in a large system. It dominates only very near to threshold.) In two dimensions, which we have studied most extensively, we find  $\gamma = 1.8 \pm 0.15$  and  $\gamma_\ell^I = -0.40 \pm 0.12$ .

When the force is decreased from  $F_T^+$ , initially no jumps occur and the minimum of  $\mathcal{H}$  evolves smoothly. In this regime, which appears to persist for a finite range of  $F$  in large systems, the evolution is reversible, so that  $\chi^\uparrow = \chi^\downarrow = \chi_0$ . For this history, the field can be increased back to threshold, yielding a *reversible approach* characterized by a *cusplike*

$$\chi_0(F) \approx \chi_T - A^R (F_T^+ - F)^{-\gamma_\ell^R} \quad (1.9)$$

with  $\gamma_\ell^R = -0.42 \pm 0.05$  in two-dimensional systems. Within our error bars,  $\gamma_\ell^I = \gamma_\ell^R$  (although the amplitudes  $A^I$  and  $A^R$  differ), which is somewhat surprising in light of the large differences between the two approaches: in the irreversible approach, the linear polarizability is only a small addition to a much larger polarizability  $\chi^\uparrow$  dominated by the jumps. We propose in Sec. IV that the scaling *form* for the distribution of linear eigenmodes is independent of the approach to threshold, with a common frequency scale  $(F_T^+ - F)^\mu$ , where  $\mu \approx 0.50$ , but with history-dependent scaling functions.

### C. Finite size effects and avalanche size distribution

In order to investigate the correlation lengths which characterize the critical behavior near threshold, we study finite size effects in some detail in Sec. V and determine the avalanche size distribution for the irreversible approach to threshold. In general, one expects the singular properties of large finite size systems to exhibit finite-size scaling behavior as functions of  $L/\xi$ , with  $\xi$  the correlation length. For example, the polarization density on the irreversible approach to threshold is expected to behave as

$$P_{\text{sing}}^\uparrow(F, L) \approx (F_T^+ - F)^{-\gamma} \Phi^\uparrow(L/\xi). \quad (1.10)$$

Here, however, because of the randomness and existence of a threshold in finite systems, care must be taken to use the appropriate sample specific finite system quantities, as we see

in Sec. V.

From the polarizability  $\chi^\uparrow$  on the irreversible approach, as well as the width of the distribution of threshold fields, we find a correlation length

$$\xi \sim (F_T^+ - F)^{-\nu} \quad (1.11)$$

with  $\nu = 2.01 \pm 0.02, 1.01 \pm 0.03$  in  $d = 1, 2$  respectively. To within our errors,  $\nu$  seems to saturate the inequality  $\nu \geq 2/d$  [16].

The divergence of  $\xi$  is in agreement with the divergence of the measured characteristic size of avalanches as threshold is approached. At threshold, the distribution of avalanche sizes is scale-invariant, with a distribution quite similar to that seen for sand-pile models of the same dimensionality ( $d = 2$ ). The CDW model is clearly not “self-organized”, as the scale-invariant behavior is seen only at threshold. The apparent connection between the two models is quite interesting, though, and it is briefly developed below.

One can also investigate finite size corrections to the polarizability in the reversible approach to threshold. Surprisingly, these are characterized by a distinct characteristic length

$$\xi_l \sim (F_T^+ - F)^{-\nu_\ell} \quad (1.12)$$

with  $\nu_\ell \approx 0.44 \pm 0.05 < \nu$  in  $d = 2$ . The origin of this second length, which naively violates the inequality for  $\nu$ , is quite subtle. It is connected to the effects of the smooth potential and the absence of a natural connection (such as a magnetic field in conventional equilibrium phase transitions) which links one side of the transition to the other. If the polarizability in the reversible approach is scaled with the dominant correlation length  $\xi$ , there will be *no finite size corrections to  $\chi_0$ !*

In the last section of this paper, we discuss the finite size lengths and related issues, consider some possible scaling laws, and raise questions for future work. A summary of our numerical results for critical exponents is presented in Table I. The error bars for the exponents are subjective, except for  $\nu_T$ , where the error bars are statistical, and reflect the



range of values which are consistent with the data in the appropriate scaling regime (see figures and discussion in each section).

#### D. Related models

Before proceeding with a more detailed discussion of the CDW model of Eq. (1.2), we first define several other models to which we compare some of our results.

In the limit that the range of interactions in Eq. (1.2) becomes infinite range, mean field theory becomes valid, and one can replace  $z^{-1} \sum_{\delta} \varphi_{i+\delta}$  (with  $z = 2d$  the coordination number), by a self-consistently calculated mean field  $\bar{\phi}(t)$ , so that the  $\Delta\varphi_i$  term of Eq. (1.2) is replaced by  $\bar{\phi}(t) - \varphi_i$ . This model has been studied in some detail in Ref. [4] and shows some features qualitatively similar to the present finite dimensional results, particularly the presence of reversible and irreversible approaches to threshold and the spectrum of local soft modes.

A one dimensional incommensurate version of Eq. (1.2) has also been studied [17]. Here the interactions are nearest neighbor, but the pinning phases  $\{\beta_i\}$  are chosen to be quasiperiodic (rather than random), i.e.,  $\beta_i = 2\pi\alpha i$ , with  $\alpha$  an irrational, usually chosen to be the golden mean. For  $h$  greater than a critical value  $h_c$ , this system exhibits a non-zero threshold somewhat similar to the random system.

Finally, several authors have studied [18,19] a simple “random friction” model, in which the cosine pinning potential is (essentially) replaced by a periodic sawtooth with

$$V_i(\varphi_i) = h_i\varphi_i \quad \text{for} \quad \beta_i > \varphi_i > 2\pi - \beta_i, \quad (1.13)$$

and  $h_i$  random with some distribution;  $V_i$  is periodic with period  $2\pi$ . The discontinuity in  $V_i$  at  $\beta_i$  does not affect the steady state dynamics of the moving phase, but only stops the phases from “backsliding” below threshold. At threshold, the distortion of the phases in this model can be calculated directly, as can the distribution of threshold fields. The threshold field  $F_T(\{h_i, \beta_i\})$  is simply the average of  $h_i$  over the system, so that in a system of size  $L^d$ ,

the width of the distribution of threshold fields is  $\Delta F_T(L) \sim L^{-d/2}$ . The mean distortions at threshold (and for all fields above threshold) behave as

$$\overline{(\varphi_i - \varphi_j)^2} \sim |i - j|^{(4-d)/2} \quad (1.14)$$

for  $d < 4$ , since the discontinuities in the potential do not play a role (we note that a “ratcheted kick” model [3], where the phase is advanced by a finite amount when it reaches a discontinuity, has much more complicated behavior above threshold; see Sec. VI).

## II. ANALYTIC BOUNDS

The behavior of CDW’s below threshold is characterized, as discussed above, by many locally stable configurations and concomitant hysteresis. Above threshold, the many nonlinearly interacting degrees of freedom might be expected to lead to strong sensitivity of the motion to initial conditions, aperiodicity, or non-uniqueness. As one of us has shown elsewhere [3], however, the convexity of the interactions between the phases assures that at long times, CDW’s above threshold approach a *unique periodic* steady state (as seen in numerical simulations [11–13]). In this section, we show that similar convexity arguments lead to a partial ordering of the configurations below threshold, bounds on the motion, and the uniqueness of the configuration *at* threshold.

### A. The no-passing rule

The central result upon which these conclusions are based is what we call the “no-passing” rule. This rule severely restricts the behavior of solutions to the equation of motion. Suppose one has two solutions to the equation of motion Eq. (1.2), for the same realization of the pinning and same drive field. If the initial conditions are such that the values of all the phases for one solution (the “greater” solution) exceeds the phases in the other solution (the “lesser” solution) at each point in space, the greater solution can never be “passed” by the lesser one (see Fig. 1). Physically, if the phases of the two solutions approach each other

at some site, the pinning and drive forces cancel, but the elastic forces due to neighboring sites keep the phases from passing through each other, since the elastic forces tend to flatten out the configuration. This rule, though quite simple and easily derived, provides a partial ordering for the stationary solutions to the equations of motion and directly implies that the velocity is a unique function of the applied field.

We now justify this rule in more detail. Consider two solutions to the equations of motion Eq. 1.2,  $\{\varphi_i^1(t)\}$  and  $\{\varphi_i^2(t)\}$ , for the same realization of the disorder  $\{\beta_i\}$ , with initial conditions chosen so that  $\varphi_i^1(0) < \varphi_i^2(0)$ , for all  $i$ . We will say that such a configuration  $\{\varphi_i^1(t)\}$  is *less than*  $\{\varphi_i^2(t)\}$  at  $t = 0$ . Each set of phases is driven by the same, possibly time dependent, external field,  $F(t)$ . Define the differences

$$\epsilon_i(t) = \varphi_i^2(t) - \varphi_i^1(t). \quad (2.1)$$

Subtracting the equations of motion Eq. (1.2) for the two solutions gives

$$\frac{d\epsilon_i(t)}{dt} = \Delta\epsilon_i(t) + h \left[ \sin(\varphi_i^1 + \epsilon_i - \beta_i) - \sin(\varphi_i^1 - \beta_i) \right]. \quad (2.2)$$

Let  $j(t)$  be a site where  $\epsilon$  is equal to its minimum value. Since  $\Delta\epsilon_{j(t)}$  is non-negative and the second term of Eq. (2.2) is bounded in magnitude by  $h|\epsilon_i|$ ,

$$\frac{d}{dt}\epsilon_{j(t)} > -h\epsilon_{j(t)}(t). \quad (2.3)$$

It follows that  $\epsilon_{j(t)}(t)$  decays no faster than exponentially to zero (indeed it will often increase) and therefore, for all  $i$ ,  $\varphi_i^1$  cannot coincide with or cross  $\varphi_i^2$  at any time (in the sliding state,  $\min_i(\epsilon_i)$  is bounded below by a constant which depends on the initial configurations  $\varphi_i^1, \varphi_i^2$  [3]). Thus we conclude that if  $\{\varphi_i^1(0)\}$  is less than  $\{\varphi_i^2(0)\}$ ,  $\{\varphi_i^1(t)\}$  will be less than  $\{\varphi_i^2(t)\}$ , for all  $t > 0$ .

It is clear that this no-passing rule relies crucially on the elastic potential between sites being convex. Note that for models where the elastic potential is not convex, this result does not hold, and, in fact, many of the conclusions that we will derive here do *not* hold for models with phase slip [20].

## B. Consequences of no-passing

The no-passing rule has several immediate, useful consequences. The first is the uniqueness of the velocity. Suppose there are two solutions to the equations of motion in a finite system, for the same field  $F(t)$  and pinning realization  $\{\beta_i\}$ . By discrete translation invariance of the equations of motion by multiples of  $2\pi$ , either of the two solutions initially can be translated to become a lesser solution. By the no-passing rule, the average velocity of the lesser solution is bounded above by that of the greater solution. Since the choice of initially lesser configuration is arbitrary, all solutions to the equations of motion in finite systems must have the same velocity, in the limit of long times.

This immediately implies that the threshold field is unique, since moving solutions cannot coexist with stationary solutions. The threshold configuration itself is almost always unique. Since the pinning potential is random, generically no more than one minimum will disappear simultaneously at  $F_T$ . The last stationary solution to disappear as  $F$  increases is thus, with probability one, the unique threshold configuration, modulo uniform  $2\pi$  shifts of all the phases.

Another important consequence of the no-passing rule is the bounding of the motion for fields  $F$  in the static range,  $F_T^- \leq F \leq F_T^+$ . This bound shows that, given an initial configuration and for monotonic changes in the field, the final configuration approached depends only on the final field. In particular, the final configuration is independent of the rate of change of the applied field. This allows for a natural ordering of the static states which is useful for understanding hysteresis and for the simulation of the model (see Sec. III).

Consider any particular realization of the pinning  $\{\beta_i\}$ . Let  $\{\varphi_i(t)\}$  be a solution to the equations of motion Eq. (1.2) for a (possibly) time-dependent field  $F(t)$  which is bounded above by a constant  $F^*$ , with

$$F(t) \leq F^* \leq F_T^+, \quad (2.4)$$

for all  $t$ . Define  $\mathcal{A}^*(\{\varphi_i(0)\})$  as the set of all configurations  $\{\varphi_i^*\}$  that are stationary at the field  $F^*$  and that are greater than the initial configuration, i.e.,  $\varphi_i(0) \leq \varphi_i^*$ , for all  $i$ .

Suppose that the configuration  $\{\varphi_i^*\}$  is a member of  $\mathcal{A}^*$ . The “no passing” rule implies that  $\varphi_i(t) \leq \varphi_i^*$ , for all  $t > 0$  and all  $i$ ; as the initial configuration evolves, it cannot pass any configuration  $\{\varphi_i^*\}$  that is both stationary at the bounding field  $F^*$  and greater than the initial configuration. Fig. 2 schematically shows some of the configurations  $\{\varphi_i^*\} \in \mathcal{A}^*$ . If the field  $F(t)$  is non-decreasing in time, with  $F^* = \lim_{t \rightarrow \infty} F(t)$ , then  $\{\varphi_i(t)\}$  approaches a stationary configuration defined by  $\varphi_i^\infty = \lim_{t \rightarrow \infty} \varphi_i(t)$ . This limit configuration is stationary at field  $F^*$  and is greater than the initial configuration  $\{\varphi_i(0)\}$ , therefore it belongs in the set  $\mathcal{A}^*$ . The configuration  $\varphi_i^\infty$  is the *least* configuration that is greater than  $\{\varphi_i(0)\}$  and stationary at  $F^*$ : it has the property that  $\varphi_i^\infty \leq \varphi_i^*$  for all  $\{\varphi_i^*\} \in \mathcal{A}^*$ , since the configuration  $\{\varphi_i(t)\}$  cannot pass *any* of the configurations in  $\mathcal{A}^*$ . For non-decreasing  $F(t)$ , the final configuration approached is thus *unique* and *independent* of the rate at which  $F(t)$  approaches  $F^*$ . The final configuration depends only on the initial configuration and the value of  $F^*$ . As we see below, this result enables the stationary configurations which occur for adiabatically changing  $F$  to be computed more efficiently.

### C. Other physical systems

We note that the no-passing rule and its consequences are applicable to models of other physical systems, including the motion of interfaces in random systems, e.g., fluid interfaces in porous media [21]. The two most important requirements for the no-passing rule are convex elastic interactions and the parameterization of distortions by a *single* field defined on the elastic medium. Flux flow in superconducting films, for example, fails both of these tests: the flux lattice can rearrange itself plastically under large strains (non-convex elastic forces) and there are two internal coordinates (the position vector of individual fluxoids). It has been shown [20] that models with non-convex elastic interactions can have hysteresis in the velocity vs. field relation. Note that is even possible to define *zero-dimensional* models that have two (internal) coordinates where the velocity is hysteretic [22].

### III. NUMERICAL ALGORITHMS

Previous simulations [11,12,18,23] of the lattice CDW model have used direct numerical integration of the equations of motion. Some of our results were also obtained with this method. When we used a second-order predictor-corrector method to integrate the equations of motion, we found that time steps in the range 0.05-0.1 were sufficient for finding stationary configurations (and also for simulating the sliding state). For the parameters we used, decreasing the time step did not change the results. A great disadvantage of this method is that the relaxation time to a static configuration can be quite long. This occurs when the simulation is converging towards a configuration that has soft modes (i.e., linear relaxational modes with relaxation rates  $\ll h$ ). As we shall see, such soft modes are often important. This problem, not surprisingly, is especially bothersome near threshold.

For fields in the static range, of primary interest here, we used an alternative method to find static configurations and to calculate the changes in configuration that occur when the drive field is changed. It is similar to a method previously used in the incommensurate case [17]. This method, which relies on the existence of the no-passing rule for the CDW model, is often over two orders of magnitude faster than direct numerical integration. In fact, we found this algorithm essential to achieve well-converged configurations in large systems for fields near threshold.

For an example of the method used, suppose that, using numerical integration, one has obtained an initial configuration stationary at a field  $F^0$ , and one wishes to find the configuration that is static at some greater field  $F^*$ ,  $F^0 < F^* < F_T^+$ , that would result from integrating the equations of motion, with field  $F^*$  for times  $t > 0$ . This configuration is the unique *lowest* configuration, above the initial configuration, that is static at field  $F^*$ , by the above discussion of the ordering of static states. Any algorithm that determines this lowest configuration will be an acceptable method. The method that we use is to advance each degree of freedom towards, *but not beyond*, the nearest local minimum of the local energy defined at each site  $i$ ,  $\mathcal{H}_i(\varphi_i)$ , which is determined by calculating the total energy  $\mathcal{H}$  with

all neighboring phases *fixed*.

To advance individual phases toward the minima of  $\mathcal{H}_i$ , we use a variant of the Newton-Raphson algorithm, which we modify to avoid overshooting the minima, while retaining rapid convergence. We need to find zeroes of the velocity

$$\dot{\varphi}_i = -\partial\mathcal{H}/\partial\varphi_i \equiv -\mathcal{H}'_i \equiv F_i + V'_i - 2d\varphi_i, \quad (3.1)$$

where the local field  $F_i \equiv \sum_{\delta} \varphi_{i+\delta} + F$  and the pinning force  $V'_i \equiv h \sin(\varphi_i - \beta_i)$ . Instead of the usual iterative map  $\varphi_i \rightarrow \varphi_i - \mathcal{H}'_i/\mathcal{H}''_i$ , we solve for zeroes of  $\dot{\varphi}_i$  by the map

$$\varphi_i \rightarrow \varphi_i - \mathcal{H}'_i/(\mathcal{H}''_i - c\mathcal{H}'_i), \quad (3.2)$$

where  $c$  is a constant that depends on the pinning strength [24]. After a single iteration of this map for each site, the local fields are updated. At each step, the phases only increase, and the local fields  $F_i$  increase. This map is iterated until a fixed configuration is reached, which corresponds to a stationary configuration. Since the phases never “pass” a minimum of the energy, the configuration reached is the lowest configuration, greater than the initial configuration, that is static at field  $F^*$ . The fixed configuration obtained by this method is therefore the same as would be obtained by numerical integration of the equations of motion.

The threshold fields for each particular realization of the pinning was found by bisection. Upper and lower bounds were found for the threshold field (estimated from previous runs or taken to be given by  $0 < |F_T| < h$ ), and a configuration stationary at the lower bound was found. These bounds were then improved by determining whether the configuration stationary at the lower field could be evolved, by the methods just described, into a configuration that was stationary at a trial field equal to the mean of the two bounds. If so, then the lower bound and static configuration were updated. If not, the upper bound was lowered to the trial field. Note that the no-passing rule implies that if the movement of *all* of the phases from their initial positions becomes greater than  $2\pi$  at any iteration, the applied field must be greater than the threshold field. This provides an unambiguous criterion to determine when the threshold field has been exceeded.

The computations were carried out on the 16K CM-2 Connection Machine at Argonne National Laboratories and the CM-2 at Syracuse University. For small systems, many realizations of the pinning were studied simultaneously. For all simulations, we used periodic boundary conditions. The pinning strengths  $h_i$  were taken to be uniform, as in Eq. (1.1), with values of 2.5, 5.0, and 7.5 in one, two and three dimensions, respectively. These values of the pinning strength,  $h = (2.5)d$ , were chosen to yield a Lee-Rice length  $\xi_{LR}$ , the scale at which the elastic and pinning energies are comparable [9], of approximately one lattice unit. Since regions of volume  $\xi_{LR}^d$  act effectively as single degrees of freedom, this choice allows for the most efficient simulation of many effective degrees of freedom. With these values for the pinning strength, we find the threshold fields for large systems to be  $1.338 \pm 0.004$ ,  $1.490 \pm 0.005$ , and  $1.282 \pm 0.002$  in one, two and three dimensions, respectively. That these are of order unity is consistent with the Lee-Rice length being approximately one lattice unit. (These values of the pinning strengths are also very similar to those used in Ref. [23].)

#### IV. NUMERICAL RESULTS FOR CRITICAL BEHAVIOR

In this section, we present our numerical results for the critical behavior as threshold is approached from below. As discussed in the Introduction, the behavior is strongly history dependent below threshold (this is already seen in the mean field limit [4]). We thus choose two distinct, well-defined approaches to threshold on which much of the behavior differs *qualitatively*. Nevertheless, some of the properties are quantitatively similar for these two histories, suggesting some underlying genericity. The primary quantities we study are the polarization  $P$  and various polarizabilities as defined in the Introduction.

As discussed above, the configurations at the positive and negative thresholds,  $F_T^+$  and  $F_T^-$ , are unique. Thus natural reproducible histories can be analyzed in which the field is slowly swept back and forth from  $F_T^-$  to  $F_T^+$ . The paths on approaching  $F_T^+$  and going away from  $F_T^+$  are, as we shall see, quite distinct. If  $F$  is increased to above threshold, and then decreased again slowly, the same configurations will be passed through below  $F_T^+$ , up to



uniform  $2\pi$  translations.

### A. Hysteresis and qualitative behavior

We now examine the results of a simulation of the histories, for which the initial configuration is the configuration static at  $F_T^-$ . The applied field is then varied adiabatically; first increasing to  $F_T^+$ , then decreasing back to  $F_T^-$ . Fig. 3 shows the polarization as a function of applied field for a single two-dimensional system of linear size  $L = 64$ , for this history. A similar hysteresis loop has been seen previously in simulations of the random-friction model in one dimension [18]. We use this loop to uniquely (up to translations by multiples of  $2\pi$ ) define two paths in configuration space, which are parameterized by the applied field:  $\{\varphi_i^\uparrow(F)\}$ , for field increasing from  $F_T^-$ , and  $\{\varphi_i^\downarrow(F)\}$ , for field decreasing from  $F_T^+$ .

We refer to these histories as the two “extremal” histories. For any system subject to a time dependent field  $F_T^- \leq F(t) \leq F_T^+$ , with an initial configuration belonging to an extremal history, the evolution of the configuration is bounded by this hysteresis loop:

$$\varphi_i^\uparrow(F(t)) \leq \varphi_i(t) \leq \varphi_i^\downarrow(F(t)), \quad (4.1)$$

for all  $i$  and  $t > 0$ . This result follows directly from the no-passing rule: it bounds the changes in polarization for such an initial configuration. General time-dependent configurations need not be bounded by this simple loop. However, if the applied field changes adiabatically and equals the threshold field at any time, the evolution at later times will be bounded by this loop (or uniform  $2\pi$  translations of it.)

For our choice of pinning strength, we find that the initial section of each of the extremal paths, where the field is *reduced in magnitude* from its threshold value,  $F_T^\pm$ , is *reversible*. For all quasistatic field histories that start with a configuration that is static at field  $F_T^+$  or  $F_T^-$ , the configuration is a unique function of the field for a range of fields near threshold, even if the direction of the field change is reversed. This is consistent with our observation that, over this field range, *no jumps in the phase occur*, since no local minima vanish. The

polarization is a smooth function of field over this range, even for finite systems. In two dimensions, we find the range of fields  $F_T^+ \geq F \geq F_R$  over which the system is reversible is given by  $F_T^+ - F_R = 0.80 \pm 0.03$ , while  $|F_T| = 1.490 \pm 0.005$ .

This reversibility over some range is consistent with that seen in experiments on CDW's [25], where the resistance is measured as a function of the history of the applied field. The CDW configuration affects the electrical transport properties of the normal carriers, even when the CDW is pinned. The resistance in the pinned state is therefore a useful probe of the history-dependence of the CDW configuration, though the exact correspondence between the resistance and CDW configuration is not clear. Duggan, et. al., [25] find that when the field is lowered from above threshold to some distance below threshold, there is a region where the resistance is a reversible function of the field. When the field is lowered further below threshold, hysteresis is evident, however. Qualitatively, these results are in agreement with our numerical results and with mean-field theory [4].

We have examined the critical behavior for the two approaches to the threshold value of the field,  $F_T^+$ , which are defined by the two extremal paths,  $\{\varphi_i^\uparrow(F)\}$  and  $\{\varphi_i^\downarrow(F)\}$ . One history is the *irreversible* approach, for which the initial configuration is the one static at  $F_T^-$ . The critical behavior is given by the behavior of the configurations  $\{\varphi_i^\uparrow(F)\}$  as  $F \nearrow F_T^+$  and is equivalent to the critical behavior that would be seen by sweeping the field adiabatically from large negative field towards  $F_T^+$ . The *reversible* history uses the configurations which belong to the path obtained by lowering the field from  $F_T^+$  (but not as far as  $F_R$ ) and then approaching  $F_T^+$  again. The critical behavior for this history is given by the properties of the configurations  $\{\varphi_i^\downarrow(F)\}$  near  $F_T^+$  and is statistically equivalent (by the *statistical*  $\varphi \rightarrow -\varphi$  symmetry) to increasing the field slowly from large negative fields and studying the behavior near  $F_T^-$ .

## B. Polarization at threshold

An obvious first question concerning the critical behavior below threshold is whether the polarization diverges as the threshold field is approached (for some generic field history, such as the extremal histories) in an infinite-size system. In the infinite-range model, if the range of pinning values is bounded, the polarization cannot diverge [4]. But in an infinite system in finite-dimensions, there is no constraint that prevents the polarization from diverging. However, as shown in [3], there is a strict bound on the width  $W(L) \equiv \max_i \varphi_i - \min_i \varphi_i$  of a configuration in a system of size  $L$ , if  $h$  is bounded by a constant  $h_{\max}$ .

This bound on the width,  $W(L) \leq h_{\max}L^2/2$ , gives a bound for the polarization of the threshold configuration: by the no-passing rule, some phase must move by less than  $2\pi$  for fields below threshold. The largest amount that a single phase can increase below threshold is then  $2W + 2\pi$ , since no phase may differ by more than  $W$  from another. The polarization of a configuration, relative to any static initial configuration, is therefore bounded by  $2\pi + h_{\max}L^2$ . As we now discuss, numerical calculations show that the *typical* polarization increases with  $L$  much less rapidly than this strict bound.

Fig. 4 shows our numerical results for  $P_T$ , the polarization at the threshold field  $F_T^+$ , as a function of  $L$ , the linear size of the system, in one and two dimensions. The initial reference configuration is the one static at  $F = F_T^-$ . Clearly the polarization diverges with system size in both one and two dimensions, but more slowly than  $L^2$ . At threshold, the only important length scale is expected to be  $L$ , so the simplest behavior that might be expected for the polarization at threshold,  $P_T(L)$ , is

$$P_T(L) \sim L^\rho \tag{4.2}$$

for some exponent  $\rho$ . From a fit to the data shown, we estimate  $\rho$  to be  $1.3 \pm 0.3$  in one dimension and  $0.8 \pm 0.2$  in two dimensions. We discuss this result in terms of finite size scaling in Sec. V. The variation in  $P_T$  from sample to sample appears to be of the *same order* as  $P_T$ , so it would require many samples at large sizes to obtain a precise estimate for

the exponent  $\rho$  (numerically, the r.m.s. fluctuations in  $P_T$  are approximately  $0.25P_T$  in two dimensions).

### C. Subthreshold polarization and linear response

We now consider the critical behavior of the polarization as threshold is approached with  $F \nearrow F_T^+$ . On the irreversible approach, the polarization changes by non-linear jumps, where sections of the CDW move forward in response to infinitesimal changes in the applied field, and also a linear response. Though the non-linear response is very different for the two approaches to threshold, the linear response appears to have universal features.

#### 1. Definition of reduced field

In contrast to thermodynamic transitions that occur at a critical temperature, for which fluctuations make the definition of the exact location of the transition temperature ill-defined in a finite size system, the dynamical system that describes CDW's at zero temperature has no noise and any finite system has a well-defined threshold, since the steady-state velocity is either zero or non-zero. We thus define the reduced field  $f$  relative to the threshold fields for *each realization* of the pinning:

$$f \equiv 2 \frac{F - F_T^+(h, \{\beta_i\}, L)}{F_T^+(h, \{\beta_i\}, L) - F_T^-(h, \{\beta_i\}, L)}, \quad (4.3)$$

where the threshold field  $F_T^+$  for a system of size  $L$  depends on the pinning strength  $h$  and the realization of the pinning phases  $\{\beta_i\}$ . For all realizations of the pinning, then,  $-2 < f < 0$  in the stationary phase and  $f > 0$  or  $f < -2$  in the sliding state. The reduced field  $f = 0$  strictly separates the sliding from the stationary state in each sample. This definition is necessary when averaging over many samples, since quantities such as the polarization are not defined in the sliding state, above threshold.

## 2. Irreversible approach: total response

Using this definition of the reduced field  $f$ , we have determined the polarization  $P(f)$  for the irreversible approach to the threshold field  $F_T^+$  in one and two dimensions and the reversible approach for two-dimensional systems. Figs. 5 and 6 display the results in one and two dimensions for various system sizes, for the irreversible history  $\{\varphi_i^\uparrow(F)\}$ . The polarizations are measured relative to that of the configuration static at the field  $F_T^-$ . In Fig. 7, we plot the numerical derivatives of the polarization for two-dimensional systems on a log-log scale. We define  $\chi^\uparrow = dP/dF$  as this polarizability, for the approach to threshold with *increasing* field. From this plot of  $\chi^\uparrow$  for the largest samples studied, we deduce the exponent  $\gamma = 1.8 \pm 0.15$  in two dimensions, with  $\chi^\uparrow \sim f^{-\gamma}$  for small  $f$ . For one-dimensional systems, we calculate  $\gamma$  from a fit to  $P(f)$ ; the polarization diverges as  $P \sim f^{-\gamma+1}$ . We find  $\gamma = 3.0 \pm 0.5$  in one dimension.

In three dimensions, we have not been able to determine whether the polarization diverges as  $f \nearrow 0$ , as the simulation of large three-dimensional systems requires very large amounts of computer time. We display the polarization in Fig. 8 for a  $64^3$  and a  $128^3$  system for an approach to threshold where we have used an initial configuration found by relaxing a configuration  $\varphi_i \equiv 0$  at  $F = 0$ , i.e., slightly different from the  $\varphi_i^\uparrow$  approach, giving an initial polarization  $P \approx 0$ . The polarization may be divergent in infinite systems, but only very slowly: for the  $128^3$  system, the polarization exceeds  $2\pi$  only for fields within  $\sim 0.1\%$  of threshold. This is in qualitative agreement with experimental results, where the CDW polarization is less than a wavelength of the CDW for fields approaching the threshold value [26].

## 3. Calculation of the linear response

As the field is increased adiabatically in a finite size system, the evolution of the CDW configuration is composed of intervals of smooth change that are interrupted by jumps due

to vanishing local minima of the energy  $\mathcal{H}$ . In the intervals between jumps, one can define a *linear* differential polarizability,  $\chi_0 \equiv \langle \eta_i \rangle_i$ , where  $\eta_i$  is defined as the *linear* response,  $\eta_i = \partial \varphi_i / \partial F$ , to a spatially uniform perturbation in the drive field. This linear polarizability is the zero frequency *limit* of the polarizability,  $\chi_0 = \chi(\omega \rightarrow 0)$ , since the jumps are part of the zero frequency response  $\chi(\omega = 0)$  [4]. This response is found numerically by taking the derivative with respect to the drive field  $F$  of Eq. (1.2) for a metastable state (where  $\dot{\varphi}_i = 0$ ):

$$\Delta \eta_i + h \cos(\varphi_i - \beta_i) \eta_i = -1. \quad (4.4)$$

Given a static configuration  $\{\varphi_i\}$ , we determine the  $\eta_i$  by iterative solution of the diffusion equation [27], Eq. (4.4), by iterating the map

$$\eta_i \rightarrow \left( \sum_{\delta} \eta_{i+\delta} + 1 \right) / [2d - h \cos(\varphi_i - \beta_i)], \quad (4.5)$$

until the fixed point is reached.

#### 4. Divergences due to jumps

Fig. 9 is a plot of the linear polarizability  $\chi_0$  and polarization  $P$  for the irreversible history over a small range of reduced field for a single sample of size  $128^2$ . This fine field scale allows the individual jumps in the polarization and corresponding divergences in the linear polarizability to be clearly seen. At the point where a metastable configuration vanishes, the polarization jumps a small amount due to the rearrangement of the phases in some region. For the range of fields shown in Fig. 9, the rearrangement occurs in regions of a scale of several lattice constants, resulting, at least well below  $F_T$ , in a change of the average polarization  $P$  of order  $L^{-d} \sim 10^{-4}$ .

As the metastable configuration approaches a saddle node bifurcation at a field  $f_{\text{jump}}$ , where the local minima of the energy vanishes, the linear polarizability from the local degrees of freedom that go unstable diverges as  $(f_{\text{jump}} - f)^{-1/2}$ . This divergence leads to the spikes

apparent in the linear polarizability plotted in Fig. 9. As the size of the system is increased, these jumps must occur more frequently. In the thermodynamic limit, these jumps occur on a set *dense* in the applied field. The question arises, then, as to whether the linear polarizability is well-defined for the typical irreversible approach to threshold. Surprisingly, the answer is yes. The contribution to the *bulk* linear polarizability from a single degree of freedom in a sample of volume  $L^d$  is [28]

$$\Delta\chi_0 \sim L^{-d}(f_{\text{jump}} - f)^{-1/2}. \quad (4.6)$$

For a given reduced field  $f$ , the number of jumps that occur in a small field interval must be proportional to the volume  $L^d$  (for  $L$  large enough that the finite size effects discussed below are unimportant at reduced field  $f$ ). It follows that the expected distance between jumps (avalanches) is  $\Delta f \sim n_{\text{av}}^{-1}L^{-d}$  for an avalanche density  $n_{\text{av}}(f)$  ( $n_{\text{av}}(f)$  is discussed in more detail in Secs. V,VI below). At a given field reduced field  $f$ , the probability,  $p$ , that  $\Delta\chi_0 > \epsilon\chi_0$ , for some desired small relative accuracy  $\epsilon$ , behaves as

$$p \sim (\epsilon\chi_0)^{-2}[n_{\text{av}}(f)]^{-1}L^{-d}. \quad (4.7)$$

Thus, with probability  $(1 - p)$  approaching 1 as  $L \rightarrow \infty$ ,  $\chi_0$  is *not affected* by the divergences due to local degrees of freedom going unstable, to arbitrary accuracy  $\epsilon$ . We can therefore examine the nonlinear polarizability,  $\chi^\dagger$ , which includes the jumps, and the linear polarizability,  $\chi_0$ , *separately*; both are well-defined. To study the linear polarizability for the irreversible history, we examine the *median*  $\chi_0$ , which, for an ensemble of a large number of large systems, will have only a small probability of being affected by the spikes in the linear polarizability. (In principle, the above argument implies that the mean  $\chi_0$  could have been used, but the convergence as  $L \rightarrow \infty$  would be worse.)

### 5. Critical behavior of linear polarizability

We have calculated the linear polarizability for both the reversible and irreversible paths in two dimensions. For the reversible path  $\{\varphi_i^\dagger\}$ , we find that  $\lim_{f \rightarrow 0} \lim_{L \rightarrow \infty} \chi_0(f) = \chi_T$ ,

where the threshold polarizability  $\chi_T$  is a *finite* constant. The behavior near threshold of  $\chi_0(f)$  shows only a power-law cusp. This is in marked contrast with finite systems, where  $\chi_0$  diverges as  $|f|^{-1/2}$ . In order to examine the leading cusp singularity in  $\chi_0$  for the reversible approach to threshold, it is better to calculate  $d\chi_0/dF$ , as the extrapolated constant  $\chi_T$  is then unimportant. We calculate  $d\chi_0/dF$  directly by solving a linear response equation similar to Eq. (4.4), rather than by finding the numerical derivative of  $\chi_0$ . We plot the mean of  $d\chi_0/dF$  in Fig. 10, for systems of sizes  $32^2$ ,  $64^2$ ,  $128^2$ , and  $256^2$ . We define  $\gamma_\ell^R$  as the exponent determining the singularity in  $\chi_0$  for the reversible path, as  $f \rightarrow 0$ :

$$\chi_0(f) = \chi_T - A^R |f|^{-\gamma_\ell^R}. \quad (4.8)$$

We find that, for the larger systems, the data for  $d\chi_0/dF$  is well fit by the form

$$d\chi_0/dF \sim |f|^{-\gamma_\ell^R - 1} \quad (4.9)$$

over more than one decade, with  $\gamma_\ell^R = -0.42 \pm 0.05$ . The coefficient  $A^R$  is also determined by the fit to the data for  $d\chi_0/dF$ . Using the fitted quantities  $A^R$  and  $\gamma_\ell^R$  for the reversible path, we estimate

$$\chi_T \simeq \lim_{f \rightarrow 0} [\chi_0(f) + A^R |f|^{-\gamma_\ell^R}] \approx 0.483 \pm 0.005 \quad (4.10)$$

for  $d = 2$  and  $h = 5$ .

For the irreversible path, the large-volume limit of the derivative of the linear polarizability,

$$\lim_{L \rightarrow \infty} d\chi_0(F)/dF, \quad (4.11)$$

is *not* well-defined, by an argument similar to that given in Eqs. (4.6) and (4.7). To determine the behavior of  $\chi_0(f)$  as  $f \rightarrow 0$  for this path, we cannot take the derivative, as we did for the reversible path, but must examine  $\chi_0(f)$  directly. If a fit is done directly, allowing  $\chi_T$  to vary, the leading singularity cannot be determined precisely. Instead, we use the value of  $\chi_T$  which has been calculated from the reversible path. This analysis assumes that



$\chi_T = \lim_{f \rightarrow 0} \lim_{L \rightarrow \infty} \chi_0(f)$  is the same for both paths. This assumption is consistent with the data; neither the reversible or irreversible linear polarizability diverges and they are both increasing, with both paths approaching the unique threshold configuration [29]. We then fit to the form  $\chi_0(f) = \chi_T - A^I |f|^{-\gamma_\ell^I}$ , where  $A^I$  and  $\gamma_\ell^I$  are the coefficient and exponent that describe the leading singularity in  $\chi_0$  for the irreversible path. We plot  $\chi_T - \chi_0$  for both the reversible and irreversible path in Fig. 11. The uncertainties in  $\chi_T - \chi_0$  are larger for the irreversible path because of the divergences in  $\chi_0$  at the jumps. As mentioned above, we take the median value for  $\chi_0$  on the irreversible path, as the mean would poorly characterize the typical value for  $\chi_0$ . Our resulting best estimate for  $\gamma_\ell^I$  is  $-0.40 \pm 0.12$ . The exponents  $\gamma_\ell^{(R,I)}$  agree to within our error, though the coefficients  $A^{(R,I)}$  are different for the two histories. This numerical agreement suggests a universality for the singularity in the linear  $\chi_0$ , which we now examine in more detail.

#### D. Linear response: eigenmodes

We next investigate more generally the linear response about a stationary configuration. The linear response  $\chi_0$  can be expressed as the sum of contributions from the eigenmodes of the operator acting on  $\eta$  on the left-hand side of Eq. (4.4), i.e., the operator for the linear relaxation of a perturbed configuration [13,17]. For a particular configuration  $\{\varphi_i\}$ , we define eigenmodes  $a_i^m$ , with eigenvalues  $-\Lambda_m$ ,  $m = 0, \dots, N-1$ , such that

$$-\Lambda_m a_i^m = [\Delta a^m]_i + h \sin(\varphi_i - \beta_i) a_i^m. \quad (4.12)$$

We take the eigenfrequencies to be ordered so that  $0 < \Lambda_0 < \Lambda_1 < \Lambda_2 < \dots$ . The polarizability is determined by the relation

$$\chi_0 = L^{-d} \sum_{m=0}^{N-1} (\sum_i a_i^m)^2 / \Lambda_m. \quad (4.13)$$

The sum over lattice sites,  $\sum_i a_i^m$ , gives the sum of the components of the eigenvectors, which have been normalized so that  $\sum_i (a_i^m)^2 = 1$ .

We have calculated numerically the smallest eigenvalues,  $\Lambda_m$ , for  $m = 0, \dots, 5$ , in a two-dimensional system of size  $128^2$  for the *reversible* extremal history near threshold. We find that the low lying eigenmodes are *localized*: the components of the eigenmodes are very small outside of a region of size several times the lattice spacing. As the threshold is approached, *the localization length of the lowest mode approaches a constant  $\approx 1.5$*  (where the localization volume is estimated by the square of the sum of the components of the normalized eigenmode). The smallest eigenvalues appear to behave as

$$|\Lambda_m| \sim (f_m^c - f)^\mu \quad (4.14)$$

for small  $f$ , with  $\mu = 0.50 \pm 0.01$ , and  $f_m^c$  discussed below, as shown in Fig. 12. Similar results have been found in calculations for the one-dimensional model with random and incommensurate pinning phases [13,17]. This result is in agreement with a natural picture of the low-lying eigenmodes consisting of *localized, almost independent degrees of freedom*. Each eigenmode approaches a saddle-node bifurcation at a field  $F_T^+ + f_m^c$ , with  $f_m^c > 0$  for  $m > 0$ . In this picture,  $\mu = 1/2$  exactly, consistent with our numerical results. At the threshold field, the smallest eigenvalue,  $\Lambda_0$ , goes to zero (i.e.,  $f_0^c = 0$ ), with the last minimum of the energy  $\mathcal{H}$  becoming unstable. The magnitude of the other eigenvalues appear to go to zero at the reduced fields  $f_m^c$  indicated, but since the lowest mode has gone unstable and the configuration is sliding for  $f > 0$ , the linear analysis clearly no longer applies.

Since the eigenmodes are localized at threshold, the leading singular behavior can not come from the sum of the components of the lowest eigenmode, but rather arises from the singularities in the eigenvalue distribution for small  $\Lambda$ . The matrix element  $(\sum_i a_i^m)^2$  in Eq. (4.13) can be approximated by an average size,  $b$ , which approaches a constant as  $\Lambda_m \rightarrow 0$ . The singular part of the linear polarizability is then given by [13,17]

$$\chi_0^{\text{sing}}(f) \sim b \int d\Lambda \rho(\Lambda, f)/\Lambda, \quad (4.15)$$

where  $\rho(\Lambda, f)$  is the density of eigenvalues at reduced field  $f$ .

For the incommensurate model in one dimension, numerical data suggest that the eigenvalues  $\Lambda_m$  obey the scaling form [17]

$$\Lambda_m \sim |f|^\mu D(m |f|^{-\delta}), \quad (4.16)$$

with  $\mu \approx 0.50$  and  $\delta \approx 0.18$ ; for incommensurate pinning, the scaling function  $D$  is not continuous and is invariant only under discrete rescalings. The exponent  $\mu$  is interpreted as determining the frequency of the softest modes (“active regions”) near the depinning transition. The exponent  $\delta$  describes the scaling of the density of these regions. These exponents yield the dependence on frequency  $\omega$  of the ac conductivity  $\sigma(\omega)$  at threshold to be  $\sigma(\omega) \sim \omega^{\delta/\mu}$ , consistent with numerical results for the incommensurate model [17].

For a continuous distribution of eigenvalues  $\rho(\Lambda, f)$ , this scaling form can be rewritten as a scaling form for the density of states  $\rho(\Lambda, f) = dm/d\Lambda$  by solving Eq. (4.16) for  $m$  and differentiating. The result is

$$\rho(\Lambda, f) \sim \Lambda^\alpha \hat{\rho}(\Lambda |f|^{-\mu}), \quad (4.17)$$

where  $\alpha = (\delta - \mu)/\mu$  and the scaling function  $\hat{\rho}$  approaches a constant as its argument becomes large. The exponent  $\alpha$  defines the distribution of the modes at threshold ( $f = 0$ ) for small eigenvalue  $\Lambda$ . The exponent  $\mu$  characterizes the frequency scale at which the distribution of modes for  $f < 0$  differs significantly from the threshold distribution. This is a plausible form for the form of the density of states, especially for the reversible path. If the field is lowered from its threshold value by a small amount, the configuration will change very little and the only modes which will have significantly different eigenvalues will be those modes which are the softest at threshold. This scaling form is certainly consistent with our results for the behavior of the individual eigenmodes as  $f \rightarrow 0^-$  for the reversible path in two dimensions. For this reversible path, we thus expect  $\hat{\rho}(u) = 0$  for  $u$  less than a value  $u_c$ , indicating the absence of modes with frequencies less than  $u_c |f|^\mu$ . We now investigate the consequences of assuming this scaling *form* for the density of states for *both* histories, albeit with different scaling *functions*.

The scaling relation Eq. (4.17), taken together with Eq. (4.15), determine the form of the linear polarizability for small  $f$  on the reversible path. From Eq. (4.17), the singular part of the linear polarizability has the form

$$\chi_0^{\text{sing}}(f) \sim f^{\mu\alpha}, \quad (4.18)$$

implying the scaling relation

$$\gamma_\ell = -\mu\alpha. \quad (4.19)$$

In two dimensions, this scaling relation implies, given our computed values of  $\mu$  and  $\gamma_\ell$ , that  $\alpha = 0.84 \pm 0.12$ . Since  $\alpha$  is defined by the distribution of states at threshold, which is independent of history, the numerical agreement of the exponents  $\gamma_\ell^I$  and  $\gamma_\ell^R$  suggests that the exponent  $\mu$  is the same for the two histories; it is presumably exactly  $1/2$ . Of course, the scaling function  $\hat{\rho}$  is different for the two histories.

Fig. 13 schematically shows the density of states for the two paths that we have examined. From the observation that  $\Lambda_m \sim (f_m^c - f)^\mu$  for small  $f$  on the *reversible path*, it can be seen that there is a gap of size  $f^\mu$  in the density of states for configurations on the reversible path. In Ref. [4], it is argued that, for configurations along the *irreversible path*, a density of states that is *linear at small*  $\Lambda$  is stable to changes in the field. These considerations lead us to speculate that the density of states for the irreversible and reversible approaches to threshold are as shown in Fig. 13. We conclude that although the two histories have very different densities of states at the same field, due to the difference in their scaling functions  $\hat{\rho}$ , there is a common underlying frequency scale defined by  $f^\mu$ , which, with the distribution of eigenmodes at threshold, characterized by the exponent  $\alpha$ , determines the singularity in the linear response.

## V. FINITE-SIZE EFFECTS AND AVALANCHES

In the study of conventional thermodynamic transitions, the concept of a dominant diverging length scale, the correlation length, plays a crucial role in the understanding of scaling relations and the physical description of the system. Likewise, correlation lengths for some deterministic dynamical systems [30,31] have provided insight into the behavior of those models. In order to better understand the nature of the CDW depinning transition,

it is important to develop an understanding of the characteristic length(s). For CDW's, there have been some attempts to understand the correlation length in the sliding state numerically [12,23,32] and there has been some success very recently in expanding about mean-field theory in  $d = 4 - \epsilon$  dimensions [15]. These results do not, however, address the static behavior in the pinned phase.

In this section, we address the question of the definition and behavior of correlation lengths in the static regime for the lattice CDW model with random pinning phases. We define a finite-size-scaling length using the distribution of threshold fields and determine the corresponding finite-size-scaling exponent  $\nu_T$ , which we find to be very close to  $2/d$  in both one- and two- dimensional systems. We also give numerical results on finite-size scaling of the polarization for the irreversible path; from these, we determine an exponent  $\nu_n$  which describes the finite-size crossover for the polarization which is, within numerical accuracy, equal to the value for  $\nu_T$ . The sizes of “avalanches”, which occur when a local mode becomes unstable, are found to have a maximum typical size that diverges in a fashion consistent with that given by  $\nu_T$  and  $\nu_n$ . By contrast, the finite-size crossover for the *reversible* polarizability scales very differently in two dimensions, with an exponent  $\nu_\ell = 0.44 \pm 0.05$ . We discuss these relationship of these results and their connection with the bound  $\nu_f \geq 2/d$ , for finite-size-scaling exponents  $\nu_f$ , proved by Chayes, *et al* [16].

### A. Finite-size scaling

We first briefly review the theory of finite-size scaling, which has been very useful for the numerical study of conventional critical points [33]. Suppose that in an infinite system, some quantity  $Y$  scales as  $Y \sim \delta^{-y}$ , where  $\delta$  is the reduced control parameter, which goes to zero at the critical point, and the exponent  $y$  describes the critical behavior for  $Y$ . In a *finite* system of linear size  $L$  much larger than any microscopic length, the finite-size scaling hypothesis states that

$$Y(\delta, L) = |\delta|^{-y} \Psi(L\xi^{-1}), \quad (5.1)$$

where  $\xi \sim |\delta|^{-\nu}$  is the correlation length and  $\Psi$  a universal scaling function which can, however, depend on the type of boundary conditions. We consider only periodic boundary conditions, which are the simplest. Given data on the behavior of  $Y(\delta, L)$ , the exponents  $\nu$  and  $y$  can be extracted by finding values of these exponents for which a scaling plot of  $Y|\delta|^y$  vs.  $L|\delta|^\nu$  yields (asymptotically) a single curve. In this section, we apply such a finite-size-scaling analysis to the study of static properties of CDW's as  $F_T$  is approached from below.

For disordered systems, a finite-size-scaling length can be defined in terms of the statistical properties of a large number of finite-size samples [16]. Such a length can be defined by the behavior of the probability of a finite-size-scaling event; the occurrence of such an event in each sample depends on the realization of the disorder for that sample and the value of the disorder parameter. For example, in a bond-percolation model a finite-size-scaling event may be defined as the existence of a path of bonds that connects two sides of a finite-sized system: in large samples the probability of such a path existing varies rapidly with the bond probability  $p$  near the percolation threshold  $p_c$ . The scaling of the probability distribution for this event defines a finite-size length scale. In Ref. [16], it is proven that, when the transition occurs at a non-trivial value of the disorder parameter, the exponent  $\nu_f$  for the divergence of such a finite size scaling length must satisfy the bound  $\nu_f \geq 2/d$ .

It is important to make a distinction between the *statistical behavior* of the model as a function of the different realizations of the disorder and the behavior of *a single sample*. The bound of Ref. [16] applies to the statistical behavior *only* and does not necessarily apply to the finite-size effects in a single sample, which may be very different. For example, consider the simple case of an Ising magnet at low temperatures in  $d \geq 3$  which, in an infinite-volume sample, undergoes a first order transition as the magnetic field  $H$  passes through zero. At this transition, the mean magnetization density  $m$  jumps between the values  $m_0$  and  $-m_0$ . We now introduce an independent random magnetic field  $h_i$ , at each site. In a given finite sample, an approximate transition field can be defined as the value,  $H_c(\{h_i\})$ , of the uniform

field  $H$  for which the thermal expectation of the magnetization equals zero. For a collection of finite-size samples, of size  $L^d$ , the width of the distribution over the random fields of the approximate transition fields  $H_c(\{h_i\})$  has width  $L^{-d/2}$ ; this can be seen by noting that the sample-to-sample variations in the spatially averaged random field of the samples will have variations of this magnitude. This implies a finite-size-scaling exponent  $\nu_f = 2/d$  [34].

The width of the transition in a *single* sample, on the other hand, can be defined as the range of applied magnetic fields over which the magnetization switches between some  $m_s$  and  $-m_s$ , for a given  $m_s$ , for example the range  $H(m = m_s) - H(m = -m_s)$ , with  $m_s = m_0/2$ . The width of this transition *in a single sample* scales as  $L^{-d}$ : for a range of fields  $\delta H \approx TL^{-d}$  ( $T$  being temperature), the difference in free energy between the  $+m_0$  and  $-m_0$  configurations will be  $O(T)$ , so that the thermal average  $m$  will have a magnitude considerably less than  $m_0$  for fields within this distance of the transition  $H_c(\{h_i\})$  of the *single sample*. In contrast with the finite-size effects for the *statistical* behavior, this suggests a finite-size-scaling exponent  $\nu = 1/d$  for individual samples.

## B. Threshold field distribution

The threshold field is the first quantity that is calculated for each realization in our numerical study of CDW's, and it is a natural quantity to study for finite-size effects. We examine the probability distribution of the threshold field for randomly chosen pinning phases  $\{\beta_i\}$ . For an infinite system, there should be a single value for the threshold field,  $F_T(\infty)$ , so that as  $L \rightarrow \infty$ , the probability distribution of the threshold field should approach  $\delta(F_T - F_T(\infty))$ . In finite size systems, however, due to the variations in the pinning from sample to sample, the threshold field probability distribution will have a finite width.

The threshold field averaged over many realizations of the pinning for systems of linear size  $L$ ,  $\overline{F_T}(L)$ , is plotted in Fig. 14. The average threshold field rapidly approaches a constant as  $L \rightarrow \infty$ . It is difficult to study finite size effects in the mean threshold field, as the difference  $\overline{F_T}(L) - F_T(\infty)$  is smaller than the statistical error for the largest samples. Here

we focus on the second moment of the distribution, noting the possibility that  $\overline{F_T}(L) - F_T(\infty)$  might scale *differently*.

In Fig. 15, we plot a histogram distribution for the computed values of the threshold field for 128 sample systems of size  $32^2$ . From such a sample distribution, for systems of various sizes  $L$ , we can determine an estimate for the widths of the distribution at various scales. We characterize such a distribution by computing its r.m.s. width  $\Delta F_T(L)$ .

This quantity,  $\Delta F_T(L)$ , is directly related to a finite-size-scaling length, in the sense of Ref. [16]. We choose the finite-size scaling event to be the sliding of the CDW. The width of threshold fields  $\Delta F_T(L)$  then defines a field scale over which the probability of this finite-size-scaling event changes significantly. The occurrence of this event depends on the randomly chosen pinning phases and the value of the control parameter. The parameter that controls the disorder is the pinning strength,  $h$ . If the infinite-system threshold field has a dependence on  $h$ ,  $F_T(h)$ , that is well behaved, with  $dF_T/dh \neq 0$ ,  $F$  can be taken as an equivalent parameter. Since we expect that  $F_T(h)$  is a smooth function, the finite-size-scaling exponent that we derive from  $\Delta F_T(L)$  should satisfy the bound of Ref. [16].

In Fig. 16 we plot our results for the width of the threshold field distribution  $\Delta F_T(L)$  vs. linear dimension  $L$  for one- and two- dimensional CDW's. The lines show the least-square fits to the form

$$\Delta F_T(L) \sim L^{-1/\nu_T}, \quad (5.2)$$

where  $\nu_T$  is a finite-size-scaling exponent for the transition between the static and sliding states. To ensure that the length scale that we measure is much greater than any microscopic length scale ( $\xi_o$  or the lattice spacing), we fit to systems of size  $L \geq 16$  (the fit would be much worse if the  $L = 8$  data were included). From these fits, we derive a value for  $\nu_T$  of  $2.01 \pm 0.02$  in one dimension and  $1.01 \pm 0.03$  in two dimensions. Within our statistical error, these results satisfy, and appear to saturate, the bound  $\nu_f \geq 2/d$  of Ref. [16]. In the infinite range model, the width of the distribution of threshold fields as a function of number of degrees of freedom obeys  $\Delta F_T(N) \sim N^{-1/2}$  [3]. If one naively extends this result to short-



range interactions, with  $N = L^d$ , one would obtain  $\nu_T = 2/d$ . For the “random friction” model [18], the threshold field can be calculated explicitly [19,35], and the exponent  $\nu_T$  is exactly  $2/d$ , since the threshold field is just the average of the pinning strengths. It is not at all clear how to show that a similar result should hold for the finite-dimensional CDW model; indeed one might expect a non-trivial exponent, at least in low dimensions, and it is quite possible that  $\nu_T = 2/d$  only represents an approximate value.

Recent renormalization group calculations by Narayan and Fisher [15] have found that the exponent for the distribution of threshold fields is equal to  $2/d$  to lowest order in  $d = 4 - \epsilon$ , and there is some indication that this may be true to all orders in  $\epsilon$ , but perhaps with non-perturbative corrections. An interesting open question is whether the distributions of threshold fields for large systems is Gaussian; this is probably related to the question of whether  $\nu_T = 2/d$ .

### C. Finite-size effects in polarization and polarizability

Examining finite-size effects of quantities other than the threshold field gives us a check on the results for  $\nu_T$  and allows us to investigate the possibility of the existence of more than one important length scale.

One such quantity is the polarization,  $P$ , for the *irreversible* history (i.e.,  $\{\varphi_i^\uparrow(F)\}$  near  $F_T^+$ ). As discussed earlier, the polarization in the stationary phase is bounded in a finite system. The critical divergence in the polarization of the infinite system must therefore be cutoff at some field scale, which depends on the size of the system. In Fig. 5 and Fig. 6 we plot the polarization for one- and two-dimensional systems of various sizes. Apparent in these plots is a crossover from the divergent large-system critical behavior to a finite value of  $P$ , which is plotted in Fig. 4.

We first examine the finite-size scaling in the case of *two dimensions*. We assume a scaling form for the mean polarization:

$$\overline{P} = f^{-\gamma+1} \hat{P}(L f^{\nu_n}), \quad (5.3)$$

with  $\hat{P}$  approaching a constant for large values of its argument and behaving as  $\sim x^{(\gamma-1)/\nu_n}$  for small arguments  $x$ , consistent with the observation of constant polarization at small  $|f|$ . Fig. 17 shows a scaling plot of  $\overline{P}|f|^{\gamma-1}$  vs.  $L|f|^{\nu_n}$ , for fitted exponents  $\nu_n = 1.0 \pm 0.1$  and  $\gamma = 1.8 \pm 0.1$  (where the errors are estimated by finding what values of the exponents give an unacceptable deviation from a single curve). These values are in agreement with our earlier estimate for  $\gamma$ , based on the nonlinear polarizability  $\chi^\dagger$ , and are also consistent with the numerical equality of  $\nu_T$  and  $\nu_n$ . It follows directly from the assumed behavior for the scaling form that

$$\nu_n = (\gamma - 1)/\rho, \quad (5.4)$$

where the polarization at threshold  $\overline{P}_T \sim L^\rho$ , as shown in Fig. 4. The scaling relation Eq. (5.4) is found to be satisfied by our exponents for two-dimensional systems. Note however that, for  $f < L^{1/\nu_n}$ , the sample to sample variations of the polarization are of the same order of magnitude as the mean polarization.

It is not possible to find a good fit to a single scaling form for the polarization data in one dimension. We instead estimate  $\nu_n$  by a cruder procedure, using the observation that the polarization approaches a constant at small  $|f|$ . We can define a crossover reduced field,  $f_X(L)$ , by  $P_T = P_0(f_X)^{-\gamma+1}$ , with  $\gamma$  and  $P_0$  determined from the divergent behavior of  $\chi^\dagger$  in the largest systems. This is consistent with assuming the scaling form of Eq. (5.3). From the data of Fig. 4, we thereby derive an exponent  $\nu_n$  for the finite-size effects in the polarization, using  $f_X \sim L^{-1/\nu_n}$ . Using this relation, we find that  $\nu_n = 2.0 \pm 0.5$ , in numerical agreement for our value for  $\nu_T$  in one dimension.

In Fig. 18 we plot the one-dimensional data on a scaling plot, using the above *calculated* value for  $\nu_n$ . This plot suggests a consistent explanation for the failure to find a single fit for the data of various sizes: we are not close enough to threshold to see the asymptotic scaling behavior. The larger systems appear to be approaching a single scaling form, for low fields ( $|f| < 0.1$ ), while the smaller systems seem to deviate strongly. Our large value for  $\nu_n$  implies that very large systems must be examined to see clearly the true scaling behavior.

#### D. Relation of finite-size effects

Our results for the finite-size effects of the irreversible polarization and comparison with the results for  $\nu_T$  suggest a picture for a diverging correlation length near the depinning transition characterized by an exponent  $\nu = \nu_T = \nu_n$ . As the threshold field is approached in an infinite system along the irreversible path, regions of size  $|f|^{-\nu}$  are subject to fields that exceed the threshold field for these subsystems, if they were to be considered independently. These regions slide forward some distance, but are prevented from sliding further by the subsystems where the threshold field has not been exceeded; on scales large than  $|f|^{-\nu_T}$ , the probability of the subsystem threshold being exceeded is small. There are, therefore, a series of “avalanches” which occur on length scales up to  $\xi \sim |f|^{-\nu_T}$ , as the threshold field is approached. The jumps in the polarization thus grow as the size of the avalanches grow. The polarizability and polarization on the irreversible path can thus diverge as threshold is approached in an infinite system.

In a finite system, if an avalanche of size of order the system size occurs, the whole system will start sliding. The average difference of the reduced fields at which thresholds of subsystems of size  $L$  occur is of the order of  $L^{-1/\nu_T}$ . For reduced fields of order  $L^{-1/\nu_T}$ , there will thus be a leveling off of the polarizability, as there will be no avalanches of linear size of order  $L$  in this range, but subsystems smaller than the system size will continue to depin at the same rate, as the width of the distribution of the threshold field on these length scales is much larger than  $L^{-1/\nu_T}$ . This physical picture is supported by the data of Fig. 7, where the *polarizability* appears to roughly level off at a value that increases with system size. With the polarizability approaching a constant, the polarization saturates. This is consistent with a crossover in the polarization curve at a reduced field scale given by the exponent for the threshold field distribution,  $\nu_T$ . We therefore conjecture that

$$\nu_n = \nu_T \equiv \nu. \tag{5.5}$$

We emphasize that the definition of the finite-size-scaling length for the polarization is *not* based on the scaling of the probability distribution for some finite-size-scaling event, and it

is therefore necessary to argue, as we have here, that the exponents  $\nu_T$  and  $\nu_n$  are directly related, since we cannot prove  $\nu_n \geq 2/d$  directly.

### E. Avalanches

The above argument relating avalanche size to the definition of  $\nu_T$  can be compared with the numerically calculated distribution of avalanche events. We have conducted such a calculation for a system of size  $256^2$ . Starting from the negative threshold field  $F_T^-$ , we adiabatically increase the field  $F$ , thereby following the path  $\{\varphi_i^\uparrow(F)\}$  in configuration space. At each local instability, we measure the moment  $\Delta P$ , defined as the change in polarization  $P$  from just below to just above the instability. The no-passing rule can be used to show that, for an infinitesimal change in the field, no phase may advance more than  $2\pi$ . The change in phase  $\Delta\varphi_i$  at each site during an avalanche is therefore bounded by  $2\pi$ , and the quantity  $\Delta P/2\pi$  provides a good estimate of the avalanche size, as the width of the “boundary” of the avalanche is of the order of the Lee-Rice length (qualitatively, the avalanches appear to be compact and not fractal in our simulations).

The results of this calculation are plotted in Fig. 19. Each point represents a single avalanche (event) due to a local instability (corresponding to the peaks in  $\chi_0$  and discontinuities in  $P$  shown in Fig. 9), plotted in the  $\Delta P$ - $F$  plane. According to the arguments in the previous section, there should be a scale  $\xi$  which determines avalanche sizes and diverges as  $\xi \sim (F - F_T)^{-\nu}$ . The solid line in Fig. 19 shows the expected dependence of avalanche size on field,  $\Delta P \sim (F - F_T)^{-d\nu}$ , under the assumption that  $\nu = \nu_T$  (we have added an arbitrary vertical shift in the curve). The dependence of the apparent cutoff in the measured avalanche sizes on the field is consistent with this dependence. A more detailed analysis of the cutoff length would require a greater number of events than can be feasibly obtained at this time.

To investigate the limit  $F \nearrow F_T^+$ , we find the cumulative distribution of the events contained in the region outlined by the dashed lines shown in Fig. 19. For this set of avalanches,

the cutoff length is greater than the linear size of the avalanches, and therefore these data should reflect the distribution of avalanche sizes just below the threshold field in an infinite system (we have tried several different reasonable criteria for choosing sets of avalanches near threshold, and find results independent of the exact choice). A logarithmically binned distribution of these events is shown in Fig. 20, where  $N(\Delta P)$  is the number of events in the range  $[2^{-1/2}\Delta P, 2^{1/2}\Delta P]$ . To within the statistical errors, this distribution is fit by the power law form

$$N(\Delta P) \sim \Delta P^{-\kappa/d} \quad (5.6)$$

with  $\kappa = 0.34 \pm 0.10$ . The value of this exponent is in numerical agreement with that of the corresponding distribution seen in models of self-organized criticality [7,36]. This strongly suggests that the state on approach to threshold in CDW's is closely related to the self-organized critical state seen in "sandpile" models. This is consistent with a distribution of avalanches cutoff only by the system size in the range of reduced fields  $L^{-1/\nu_T} < f < 0$  in the CDW models and a distribution of responses to perturbations similar to that seen in the sandpile models. These results suggest a possible universal behavior for the nonlinear response in systems in such critical states, whether obtained by adjusting a control parameter near threshold or by a mechanism of "self-organization". Note that the *typical* avalanche has a *non-divergent* size as  $F \nearrow F_T$ , since  $\kappa > 0$  — the diverging correlation length becomes evident only in the tail of the avalanche size distribution. The *average* avalanche size does diverge as threshold is approached, accounting for the diverging polarizability on the irreversible path (see Sec. VI below).

#### F. Effects of finite-size for the reversible path for $d = 2$

We can also define a finite-size-scaling exponent,  $\nu_\ell$ , for the crossover in the linear polarizability, for the *reversible* history. Since our value for  $\chi_T$  in the limit of an infinite-size system is an extrapolation which can only introduce error into the study of finite size effects,

we examine, as above, the derivative of the linear polarizability,  $d\chi_0/df$ , for finite-size effects. In Fig. 10, we have plotted  $d\chi_0/dF$  for several system sizes in two dimensions, averaged over several realizations for each size. In Fig. 21, we show scaled data  $(d\chi_0/dF) |f|^{\gamma_\ell^R+1}$  as a function of  $|f| L^{1/\nu_\ell}$ , to test the scaling form

$$\frac{d\chi_0}{dF} = |f|^{-\gamma_\ell^R-1} X(L|f|^{\nu_\ell}), \quad (5.7)$$

with  $X(z) \rightarrow \infty$  as  $z \rightarrow \infty$ , and  $\gamma_\ell^R$  as determined earlier. The value of  $\nu_\ell$  which gives the curves shown in Fig. 21 is  $\nu_\ell = 0.44 \pm 0.08$ .

Our numerical result for the value of  $\nu_\ell$ , which is *less* than  $2/d$ , implies that the natural definition for the finite-size length scale on the *reversible* path, does not satisfy the definition of a finite-size length scale in the sense of Ref. [16]. The distinction between the finite-size-length scale for the linear polarizability and the behavior of sample-to-sample fluctuations can be understood by examining the effects of finite-size on the linear polarizability for the reversible path.

On the reversible path, there are no hops, and no triggerings of any ‘‘avalanches’’. The configuration at reduced field  $|f| \ll 1$  is connected to the threshold configuration by a continuous path. The scaling of the threshold avalanche distribution thus does not enter. The polarizability of configurations on this path in the finite-size case can be treated as in Sect. (3.3.3), with an integral over a spectrum replaced by a sum over discrete values. It is easily seen that the polarizability of the softest mode dominates the finite-size effects. The contribution of the softest mode to the bulk polarizability  $\chi_0$  is

$$\Delta\chi_0 \sim L^{-d} |f|^{-\mu}, \quad (5.8)$$

since the softest mode goes unstable at  $|f| = 0$ . When  $\Delta\chi_0$  becomes of the same order as the singular part of  $\chi_0$ , there will be a crossover from the bulk critical behavior to *the single particle behavior*. This crossover will occur at reduced field

$$|f| \sim L^{d/(\gamma_\ell - \mu)}. \quad (5.9)$$

This implies that the finite-size-scaling exponent for the linear polarizability on the reversible path satisfies the scaling relationship

$$\nu_\ell = \frac{1}{d}(\mu - \gamma_\ell). \quad (5.10)$$

The relationship Eq. (5.10) is consistent with our numerical values for these exponents in two dimensions. The finite-size effects on the reversible path are due to the behavior of the softest mode in each sample near to *its* threshold and not the probability for some finite-size-scaling event to occur, which would depend more strongly on the realization of the disorder.

## VI. DISCUSSION

In this final section, we compare our results with those on related models and, qualitatively, with experiments on CDW's below threshold, as well as raising general questions about universality and scaling. We first recapitulate our main results.

On the irreversible approach to threshold (starting from the negative threshold), the motion of the CDW consists of smooth motion superimposed on a series of jumps or avalanches that result from the local minimum of the energy in which the system lies becoming unstable. On increasing  $F$ , the polarizability  $\chi^\dagger$  diverges with an exponent  $\gamma$  dominated by the jumps. The avalanches are initiated by *local* instabilities via simple saddle-node bifurcations (i.e., the vanishing of the eigenvalue for a localized mode), though the avalanches can be quite large, with an apparently power law distribution of their sizes extending out to the correlation length. The low frequency *linear* response in contrast is dominated by the local modes which are nearly unstable. The divergences of  $\chi_0$  at each of the local instabilities typically contributes a negligible amount in the large system limit, so that  $\chi_0(F)$  is a well-defined smooth function in this limit. In an infinite system, the zero-frequency linear response  $\chi_0$  approaches a *finite* value  $\chi_T$  at threshold with an upwards cusp characterized by an exponent  $-\gamma_\ell > 0$ ; this is in contrast to the divergence of  $\chi_0$  in a finite system at threshold.

Associated with the non-linear behavior of the avalanches, we have found evidence for a characteristic length,  $\xi \sim (F_T - F)^{-\nu}$  with  $\nu \approx 2/d$ , appearing in the width of the distribution of threshold fields in finite-size systems or the finite-size rounding of the polarization divergence. In two dimensions, this exponent is also consistent with rough estimates of the divergence of the maximum likely avalanche size as threshold is approached on the irreversible extremal path. We believe therefore that this length is the correlation length associated with the dominant physics. The exponent  $\nu$  should satisfy the bound  $\nu \geq 2/d$  and appears to be close to saturating this bound in the dimensions ( $d = 1, 2$ ) that we have studied.

We believe that the irreversible approach to threshold described above is generic in the sense that the same behavior will be found on approaching threshold from all except specially prepared initial conditions, although the *amplitudes* of the divergences in  $\chi^\uparrow$  and  $\xi$  may differ. Experimentally, the polarization on the generic approach to threshold does not exceed that given by an average CDW displacement of more than several CDW wavelengths [26,37] (a polarization by one CDW wavelength is  $P = 2\pi$  in the dimensionless units here). This is consistent with our results for three-dimensional CDW's, shown in Fig. 8.

The behavior of specially prepared initial conditions can be strikingly different from the generic behavior. When the field is reduced from threshold, there appears to be a region of finite width in  $F$  over which there are no jumps and the polarization is fully reversible, so that  $\chi^\uparrow = \chi^\downarrow = \chi_0$ . It appears quite likely that this will persist even in infinite systems, especially if the distribution of pinning strengths is bounded away from zero. As noted earlier, the qualitative features of the reversibility found in our numerical simulations is consistent with experiment [25]. Although we have not been able to find a type of rare region which would invalidate this conclusion, and our numerical evidence does not appear to indicate even logarithmic dependence on size of the lower limit of reversibility  $F_R^+$ , this conclusion should nevertheless be regarded with some caution.

In any case, the behavior of the polarizability in the reversible approach back to threshold (after  $F$  is lowered to a field above  $F_R^+$ ), is characterized by only an upwards cusp in  $\chi_0$  to



a constant,  $\chi_T$ , at threshold. To numerical accuracy, both the *value*,  $\chi_T$ , at threshold in an infinite system, and the *exponent*  $-\gamma_\ell$  characterizing the cusp, are the *same* as found for the linear polarizability  $\chi_0$  in the irreversible approach although the *amplitudes* of the cusps differ. Thus there is evidence for some degree of universality in the linear response in spite of the radical difference of the non-linear behavior in the two approaches to threshold.

This can be interpreted in terms of scaling functions for the distribution of relaxational frequencies of the linear modes which are characterized by history independent *exponents* ( $\alpha$  and an apparently trivial exponent  $\mu \approx 1/2$ ) but history dependence of the actual scaling *functions*. The reason for this behavior is somewhat of a mystery, however, because of the rather large rearrangement of the distribution of modes following avalanches as is discussed below. The finite size corrections to the linear polarizability in the reversible regime of *each particular sample* are characterized by a length which diverges more slowly than  $\xi$  with an exponent  $\nu_\ell < 2/d$ . It appears that this is *not* a true correlation length because it essentially is determined by the crossover from behavior of the large system to that of a single *localized* mode, rather than to a collective property of the whole system; it is a length related to a power of the density ( $\rho^{-1/d}$ ) of soft modes, rather than a length related to a response on large scales. Because of the existence of a sharp threshold in finite systems and the absence of a smooth connection between the pinned and moving phases, many quantities which naively appear to be characteristic lengths can occur. Similar behavior is found in other types of collective non-linear transport with a sharp threshold [38].

Before further analysis of the implications of our results, which are summarized in the Table, we first briefly compare them with those on related models.

### A. Comparison with related models

In mean field theory — valid for infinite range stiffness of the CDW — the critical behavior of the polarization depends, as in short-range systems, on the approach to threshold, but, in addition, it depends on the distribution of the pinning strengths [4]. Consider the

generic case of a distribution of pinning strengths,  $\{h_i\}$ , which is bounded below by a value  $h_0$ . If  $h_0$  is not too small, then the following behavior is found: on the first approach to threshold, the polarizability  $\chi^\uparrow$  diverges with an exponent  $\gamma > 0$  which depend on the form of the distribution of the  $\{h_i\}$ . As the field is decreased from threshold, there is a regime of reversible behavior [39] characterized by a polarizability  $\chi_0$  which goes to a constant at threshold with an upwards cusp with a non-universal exponent  $\gamma_\ell < 0$ . If the field is decreased to  $-F_T$  and then increased again, the polarizability will again diverge. Thus the behavior we have found in this paper is quite similar qualitatively to that of mean field theory, although we expect the latter to be less universal (see below).

The one-dimensional incommensurate CDW model has also been studied quite extensively [17]. Although there are again many possible approaches to threshold, the only one which has been studied is the approach from the  $F = 0$  ground state, which is reversible all the way from  $-F_T$  to  $F_T$ , a consequence of the identical pinning strengths and special symmetry. As the threshold is approached, the polarizability *diverges* with  $\gamma_\ell \approx 0.34$ . This is associated with a distribution of local relaxational frequencies the lowest of which vanishes at thresholds with an exponent  $\mu = 0.50 \pm 0.005$ , consistent, as are our data, with  $\mu = 1/2$ . Near threshold, the distribution of these frequencies has the form Eq. (4.17) with  $\alpha \approx -0.68$ . A characteristic length diverging with exponent  $\nu_\ell = \mu - \gamma_\ell$  is also found. The primary difference between this behavior and the behavior of the random  $2-d$  system studied here on its reversible approach, is associated with the sign of  $\gamma_\ell$ . In both cases,  $d\nu_\ell$  should be interpreted as the density of spatial modes with frequencies of order  $|f|^\mu$ . [For the  $1-d$  incommensurate model, there is of course no distribution of threshold fields, but the size dependence of the threshold field itself converges very rapidly, apparently faster than a power law; the interpretation of this behavior is unclear, but probably due to the nature of the best rational approximants to the incommensurate system used in the study.]

Finally we compare our present results with those of the random friction (or “ratchet”) model [18,19], which contains randomness and short range interactions, but *no jumps*.

Although this model can be solved exactly only above threshold, much of the behavior

below threshold can be guessed. A static configuration of the system consists of pinned phases which sit exactly at the ratchet positions, on which the net force (excluding the ratchet constraint) is negative, and unpinned regions with zero net force.

The distribution of threshold fields is trivially characterized by an exponent  $\nu_T = 2/d$  since  $F_T(\{h_i\}) = \langle h_i \rangle_i$  (where  $\langle \rangle_i$  denotes spatial averaging in a given configuration). Note, however, that the mean  $\overline{F_T}(L)$  is size independent. Right at threshold, the phases are just given in terms of the Fourier transform  $h(q)$  by

$$\phi(x) = \sum_q \frac{-h(q) + \langle h \rangle}{q^2} \quad (6.1)$$

so that the rms spread of phases  $\sim L^{(4-d)/2}$ . Ignoring the effects of the tail of the distribution (which probably gives rise to only  $\ln(L)$  corrections) this suggests that (for  $d < 4$ )  $P_T(L) \sim L^{(4-d)/2}$ , so

$$\frac{\gamma - 1}{\nu} = \frac{4 - d}{2}. \quad (6.2)$$

The distribution of linear sizes of unpinned regions will be cutoff above a correlation length  $\xi$  which is the size of the largest regions which have exceeded their local threshold. Thus we have

$$\nu = \nu_T = 2/d. \quad (6.3)$$

From Eq. (6.2) one obtains  $\gamma = 4/d$  [19], for a generic approach to threshold. When the field is decreased from threshold, the ratchet constraints will immediately repin some regions. The resulting singularities in  $\chi^\downarrow$  will definitely be weaker than  $\chi^\uparrow$  on a typical approach; concomitantly there will be characteristic length  $\nu_\ell < \nu$ . Further study of this non-trivial length may be useful even though the ratchet model, because of the absence of jumps, is very different on first approach to threshold from the more realistic CDW model studied here.

The values of  $\gamma$  we have found in one and two dimensions appear to be somewhat lower than the ratchet model result  $4/d$ . Nevertheless our errors are large enough not to exclude

these values. Well above threshold, the ratchet model has larger deformations than the CDW model (although they scale with the same exponent [15]). This may well also be the case at and below thresholds, perhaps leading to  $\gamma < 4/d$ .

Renormalization group calculations in  $d = 4 - \epsilon$  yield  $P_T \sim L^\rho$  with  $\rho = \epsilon/2$  to leading order in  $\epsilon$ ; this result might hold to all orders in  $\epsilon$  [15].

## B. Universality and scaling

A way to generalize the ratchet model to include jumps and make it more realistic is to replace the cosine potential in the CDW model with a sawtooth with finite slope, rather than the infinite downward slope of the random friction model. A limit of this model, called the “ratcheted-kick” model, has been studied by us above threshold, and it appears to be in the same universality class (at least as far as the dominant scaling behavior) as the cosine CDW model in two dimensions and probably also for  $d = 1$  and 3. This is *a priori* somewhat surprising since the models yield *different* dynamic exponents both in mean field theory and in zero dimensions (i.e., finite systems)!

The following conjecture is naturally suggested: *for all properties which involve the jumps, the cosine and sawtooth models are in the same universality class in low dimensions.* Thus, for example, on a generic irreversible approach to threshold,  $\gamma$  and the distribution of avalanche sizes will be the same [40].

Quantities which involve smooth evolution rather than jumps must, however, be different. Thus  $\gamma_\ell$  will be different (or nonexistent) in the sawtooth model, and there are no obvious analogs of  $\mu$  and  $\alpha$  in the sawtooth model (at least providing the modes which go unstable and trigger avalanches are localized, which, in contrast to the ratchet model, we expect them to be). Nevertheless, the density of potentially unstable regions which are destabilized by a small increase in  $\delta f$  might well be the same in both systems. In the cosine pinning model, the density of these regions diverges as  $|f|^{d\nu_\ell-1} \sim |f|^{(\alpha-1)/2}$  (using  $\mu = 1/2$ ) so that the density of modes which would be destabilized by decreasing  $|f|$  to  $|f/2|$  is  $|f|^{d\nu_\ell} = |f|^{(\alpha+1)/2}$

(for the cosine model, this is the number of modes with frequency of order  $|f|^\mu$  as noted earlier).

We thus conjecture that an exponent equivalent to  $d\nu_\ell$  or  $(\alpha + 1)/2$  can be defined for the sawtooth model and that this will be the *same* as for the cosine model in low dimensions. This certainly merits direct testing in the sawtooth model. Although the reversible regime for  $F$  decreasing from  $F_T$  should also exist for the sawtooth model, it is not clear whether  $\nu_\ell$  can be found from finite size corrections to the polarizability, since there are no obvious precursors of the local instabilities in this model.

We now discuss the conjectured universality in the context of the distribution of avalanche sizes seen in the cosine model and the rate at which avalanches are triggered. An important observation is that the distance between local regions which would be destabilized by an increase in the local driving force by of order the distance to the bulk threshold appears to be much less than the correlation length  $\xi$  (since  $\xi \sim |f|^{-\nu}$  and the distance between destabilized regions behaves as  $\sim |f|^{-\nu_\ell} \ll \xi$ ). This is even more striking if one notes that one should perhaps consider the effective increase in the force on each region as  $F$  is increased to threshold as being enhanced by the divergent polarization so that one might consider the number of regions which would go unstable if the local force were increased by  $|f/2|^{1-\gamma}$  rather than just by  $|f/2|$ . This would, however, overestimate the effects since we know (from the no-passing rule) that at least some region does not move by as much as  $2\pi$  even when  $F$  is increased all the way from  $F_T^-$  to  $F_T^+$ .

These considerations lead naturally to the consideration of the distribution of avalanche sizes near threshold. If the scaling form Eq. (4.17) for the distribution of almost unstable modes is correct in the irreversible approach to threshold, then the density of avalanches  $n_{\text{av}}$  which is triggered by a small increase  $\delta f$  is

$$n_{\text{av}}\delta f \sim |f|^{(\alpha-1)/2} \delta f. \quad (6.4)$$

Our avalanche data for the  $256^2$  system of Fig. 19 are consistent with a number of events per unit field diverging roughly as  $|f|^{-0.10 \pm 0.05}$ , consistent with Eq. (6.4). If a finite fraction of the

avalanches were of size  $\sim \xi^d$  ( $\kappa < 0$ ), then this would result in  $\gamma = (1-\alpha)/2 + d\nu = 2.10 \pm 0.09$ , which is probably an overestimate. Indeed, from the discussion in connection with the ratchet model above, we expect that in  $d = 2$ ,  $\gamma \leq 2 \leq d\nu$  (note that for  $d = 1$ ,  $\alpha$  may well be negative, as it is for the incommensurate model). This suggests that the typical avalanche is *not* of the size of the correlation length.

Given a probability distribution of avalanche sizes  $p_{av}(l, f)dl/l$ , for avalanches of linear size  $l \sim (\Delta P)^{1/d}$  at reduced field  $f$ , and the normalization  $\int_0^\infty p_{av} dl/l = n_{av}$ , we have

$$|f|^{(\alpha-1)/2} \int_0^\infty p_{av}(l, f) l^d \frac{dl}{l} \sim |f|^{-\gamma}. \quad (6.5)$$

This assumes that the typical avalanches are non-fractal, qualitatively consistent with our numerical results. A natural scaling form for  $p_{av}$ , consistent with our data, is

$$p_{av}(l, f) \sim l^{-\kappa} \Phi(l/\xi), \quad (6.6)$$

with  $\Phi(u) \rightarrow \text{const.}$  for  $u \ll 1$  and decaying rapidly for  $u \gg 1$ . In this case, we have

$$(d - \kappa)\nu = \gamma - \frac{1 - \alpha}{2}, \quad (6.7)$$

suggesting for  $d = 2$ ,

$$\kappa = 0.3 \pm 0.2, \quad (6.8)$$

consistent with our numerical result of Sec. V E. A power law decay of  $p_{av}(l, f)$  for  $l \ll \xi$  has the natural interpretation that the probability of an avalanche reaching size  $> 2l$  *given* that it is larger than  $l$  is scale invariant. If it is assumed that the exponent  $\kappa$  for the power law distribution of avalanche sizes at threshold is independent of the model, as suggested by our agreement with the distribution in models of self-organized criticality, and that  $\gamma$  is independent of the details of the model, we again reach the remarkable conclusion suggested above: that  $\alpha$ , which gives the divergence of the avalanche triggering rate as threshold is approached, is also a universal feature of CDW models.

### C. Relation to dynamics above threshold

In another paper, we will present detailed results on the dynamics of the cosine and sawtooth models above threshold. There, the steady state is a *unique* periodic function of time with period  $2\pi/v$  [3] and

$$v \sim f^\zeta \tag{6.9}$$

with  $\zeta = 0.63 \pm 0.06$  for both models in  $d = 2$  [3]. Again, for the cosine model a double finite size crossover is seen, analogous to that found below threshold in the linear polarizability. We note that a corollary of the relations proposed by Coppersmith and Fisher [17] in the 1-d incommensurate case is that  $\zeta + \nu_\ell = 2\mu$ . This relationship clearly does not hold in the  $d = 2$  random models. The jumps in the incommensurate model are correlated over the full system and a picture of locally propagating avalanches is not applicable, so that the dynamics must be described by a different picture.

For conventional phase transitions, an understanding of the scaling behavior is greatly enhanced by the addition of an ordering field which can take the system smoothly from one phase to the other. Indeed, in cases where such an ordering field *per se* does not exist — e.g., spin glasses — the understanding of the transition is far less complete.

In the case of interest here — charge density waves and related problems — it is not at all clear that a smooth connection between the two “phases” should exist, since they are so radically different, one involving no motion at all in equilibrium, but with a high degree of metastability, and the other dynamic, but unique. One possible way to connect the two phases is by adding thermal noise which will round out the threshold and yield a finite velocity for any non-zero force,  $F$ . Noise can be added in two rather different ways. The first is to add a Langevin white noise  $\eta(i, t)$  to the equation of motion, with the variance of  $\eta$  proportional to the temperature  $T$ . This will, in the stationary phase, primarily affect the modes which are near to an instability. Such an approach has been used before in mean field theory and the velocity as a function of  $T$  and  $f$  has been found to exhibit a scaling

form [4]. Numerical results and arguments based on the distribution of barrier heights in finite dimensional systems are consistent with this scaling form [6]. The exponents, however, are dependent on the form of the pinning potential, as the dependence of barrier heights on reduced field differs between smooth potentials and those with cusps. The effects of thermal noise are therefore nonuniversal.

From the above discussion of the dominance of jumps over the smooth motion, it is probably better, for examining universal properties, to add a noise which will trigger jumps in a way which depends much less on the details of the potential. The hope is that the sawtooth and cosine models will then behave similarly. We thus consider giving random “kicks” to individual phases with fixed impulse magnitude (of order  $\pi$ ) at a slow rate  $\Theta$ . For any finite  $\Theta$ , the mean velocity will be non-zero. Below threshold in the limit of infinitesimal  $\Theta$ , the mean velocity  $\langle v \rangle$  should be proportional to  $\Theta$  (provided the kicks are large enough) so that we may define a linear response

$$\Xi \equiv \left. \frac{d\langle v \rangle}{d\Theta} \right|_{\Theta \downarrow 0}. \quad (6.10)$$

Near to threshold,  $\Xi$  will presumably diverge, and above threshold,  $\langle v \rangle$  will be non-zero even at  $\Theta = 0$ , but we would again expect  $\Xi$  to be finite. Thus  $\Xi$  is somewhat like an order parameter susceptibility near a conventional thermal transition. Although we must leave investigation of this kind of noise response for future investigation, a few remarks relevant to the present paper are in order.

The main effects which cause subtleties below threshold are transients and the non-uniqueness in the absence of noise. A natural way to define, at least statistically, another type of preferred configuration at a given  $F < F_T$  is to turn on a very small noise, let the system equilibrate (if the kicks are large enough, the steady state distribution will presumably be unique, although this needs establishing), turn off the noise, let the system relax, and then study the statistical behavior of the resulting static configurations (e.g., polarizability, distribution of modes, or closeness to local instabilities, etc.). It is by no means clear, *a priori*, that such a procedure — which should be qualitatively similar to that



in real experiments — will produce configurations which are similar to *either* of the histories we have studied in this paper. If not, then it is perhaps only *transients* in the behavior above threshold and not the steady state itself which could have critical behavior related to that of, say, the irreversible approach to threshold. If, on the other hand, the configurations are statistically similar to those produced on generic noiseless approaches to threshold, then there will presumably be dynamic responses in the moving phase — such as  $\Xi$  — which can be related to exponents below threshold.

We leave these and related intriguing questions for future study.

The recent renormalization calculations of the dynamics above threshold suggest that the role of the various correlation lengths is rather different: above threshold the dominant correlation length exponent for dynamic quantities in the steady state is  $\nu_+ = 1/2$  exactly. A larger exponent  $\nu_T = 2/d + O(\epsilon^2)$  (and perhaps with no perturbative corrections) appears and controls the distribution of threshold fields. Thus the dominant length below threshold, for irreversible approaches, diverges with an exponent  $\nu_- = \nu_T$ , while above threshold dynamics is controlled by  $\nu_+ < \nu_T$ . Whether this difference is primarily due to the increased level of cooperativity in steady state above threshold, or to some other reason, is unclear. In addition, whether or not an exponent equal to  $\nu_T$  might control the dynamics far from steady state above threshold is also interesting.

Another set of questions concerns relationships to other so-called “self-organized critical” transport [7], which we have discussed above only as far as it relates to the behavior at threshold and as threshold is approached. It is plausible that such relations can also be developed in the sliding state. If CDW’s are driven at constant, very slow, *current* (i.e., fixed mean velocity) by an external field — somewhat analogous to the quasistatic limit of “sandpile” dynamics that has been extensively studied recently — then the system is near criticality and will exhibit power law correlations, etc. How the other problems studied are related to CDW’s (except in spirit and the quantitative similarities in the distribution of avalanches) is an open question: “sandpile” models typically have thermal noise (analogous to small  $\Theta$  above) but no quenched randomness. Models of earthquakes [8] with inertia but

no quenched randomness have been studied, and so have models with intrinsic randomness, but no inertia. Which are more realistic is controversial.

At this point, perhaps all that can safely be said is that the relationships between different non-linear collective transport phenomena and the possible existence of some degree of universality are likely to remain challenging problems for some time.

Acknowledgments: We thank P. B. Littlewood, S. N. Coppersmith, P. Sibani, T. Hwa, C. Myers, and O. Narayan for useful discussions. DSF is supported by the A. P. Sloan Foundation and the National Science Foundation through Grant DMR-9106237 and via the Harvard University Materials Research Laboratory. This research was conducted using the computational resources of Argonne National Laboratory and the Northeast Parallel Architectures Center (NPAC) at Syracuse University.

## REFERENCES

- [1] *Charge Density Waves in Solids*, edited by G. Hutiray and J. Sólyom (Springer-Verlag, 1985); G. Grüner, Rev. Mod. Phys. **60**, 1129 (1988); *Charge Density Waves in Solids*, edited by L. P. Gorkov and G. Grüner (Elsevier, 1989).
- [2] D. S. Fisher, in *Nonlinearity in Condensed Matter*, edited by A. R. Bishop, D. K. Campbell, P. Kumar, and S. E. Trullinger (Springer-Verlag, Berlin, 1987).
- [3] A. A. Middleton, Phys. Rev. Lett. **68**, 670 (1992); A. A. Middleton, Ph.D. thesis, Princeton University (1990).
- [4] D. S. Fisher, Phys. Rev. Lett. **50**, 1486 (1983); Phys. Rev. B **31**, 1396 (1985).
- [5] P. B. Littlewood and R. Rammal, Phys. Rev. B **38**, 2675 (1988); T. Natterman, Phys. Rev. Lett. **64**, 2454 (1990); J. Toner, Phys. Rev. Lett. **67**, 2537 (1991).
- [6] A. A. Middleton, Phys. Rev. B **45**, 9465 (1992).
- [7] C. Tang, K. Wiesenfeld, P. Bak, S. N. Coppersmith, and P. B. Littlewood, Phys. Rev. Lett. **58**, 1161 (1987); P. Bak, C. Tang, and K. Wiesenfeld, Phys. Rev. Lett. **59**, 381 (1987); C. Tang and P. Bak, Phys. Rev. Lett. **60**, 2347 (1988).
- [8] J. M. Carlson and J. S. Langer, Phys. Rev. Lett. **62**, 2632 (1989).
- [9] H. Fukuyama and P. A. Lee, Phys. Rev. B **17**, 535 (1977); P. A. Lee and T. M. Rice, Phys. Rev. B **19**, 3970 (1979); K. B. Efetov and A. I. Larkin, Sov. Phys. JETP **45**, 1236 (1977).
- [10] L. Sneddon, M. C. Cross and D. S. Fisher, Phys. Rev. Lett. **49**, 292 (1982).
- [11] L. Pietronero and S. Strässler, Phys. Rev. B **28**, 5863 (1983); H. Matsukawa and H. Takayama, Solid State Commun. **50**, 283 (1984).
- [12] N. Teranishi and R. Kubo, J. Phys. Soc. Jpn. **47**, 720 (1979); L. Pietronero and S.

- Strässler, Phys. Rev. B **28**, 5863 (1983); H. Matsukawa and H. Takayama, Solid State Commun. **50**, 283 (1984).
- [13] P. B. Littlewood, Phys. Rev. B **33**, 6694 (1986).
- [14] H. Matsukawa and H. Takayama, J. Phys. Soc. Jpn. **56**, 1507 (1987).
- [15] O. Narayan and D. S. Fisher, Phys. Rev. Lett. **68**, 3615 (1992), and preprint submitted to Phys. Rev. B.
- [16] J. T. Chayes, L. Chayes, D. S. Fisher, T. Spencer, Phys. Rev. Lett. **57**, 2999 (1986).
- [17] S. N. Coppersmith and D. S. Fisher, Phys. Rev. A **38**, 6338 (1988).
- [18] G. Mihály, M. Crommie, G. Grüner, Europhys. Lett. **4**, 103 (1987).
- [19] I. Webman, Phil. Mag. B **56**, 743 (1987); G. Parisi and L. Pietronero, Europhys. Lett. **16**, 321 (1991).
- [20] M. Inui and S. Doniach, Phys. Rev. B **35**, 6244 (1987); S. H. Strogatz, C. M. Marcus, R. M. Westervelt, and R. E. Mirollo, Phys. Rev. Lett. **61**, 2380 (1988); S. H. Strogatz and R. M. Westervelt, Phys. Rev. B **40**, 10051 (1989).
- [21] J. B. Stokes, D. A. Weitz, J. P. Gollub, A. Dougherty, M. O. Dougherty, M. O. Robbins, P. M. Chaikin, and H. M. Lindsay, Phys. Rev. Lett. **57**, 1718 (1986); M. A. Rubio, C. A. Edwards, A. Dougherty, J. P. Gollub, Phys. Rev. Lett. **63**, 1685 (1989).
- [22] In two dimensions, it is possible to define a potential with both “troughs”, which a particle can be driven along indefinitely by a field, and “pits”, where the particle will be trapped, at the same drive field. Such a potential can be used for many degrees of freedom to also obtain a hysteretic velocity-force relationship.
- [23] P. Sibani and P. B. Littlewood, Phys. Rev. Lett. **64**, 1305 (1990).
- [24] For the value of  $h = 5$  for  $d = 2$ , the constant used is  $c = 3$  and the additional condition

is imposed that no phase may increase by more than 0.3 in a single iteration.

- [25] D. M. Duggan, T. W. Jing, N. P. Ong, P. A. Lee, Phys. Rev. B **32**, 1397 (1985).
- [26] J. H. Ross, Z. Wang, and C. S. Slichter, Phys. Rev. Lett. **56**, 663 (1986).
- [27] This equation is *not* a diffusion equation in a random potential, since the  $\varphi_i$  are strongly correlated. Since there are negative values for  $h \sin(\varphi_i - \beta_i)$ , a uncorrelated distribution of these coefficients in the diffusion equation would lead to “band tails”, with positive eigenvalues, implying the instability of the solution.
- [28] G. Grüner, A. Zawadowski, and P. M. Chaikin, Phys. Rev. Lett. **46**, 511 (1981).
- [29] The divergence of the polarizability due to finite-size effects, discussed below, implies that the limit  $L \rightarrow \infty$  must be taken before the  $F \nearrow F_T^+$  limit. It is assumed here that this ordering of the limits does not affect the convergence to unique distribution of linear eigenmodes at threshold, also discussed below.
- [30] T. Bohr and O. Christensen, Phys. Rev. Lett. **63**, 2161 (1989).
- [31] D. Stassinopoulos, G. Huber, and P. Alstrøm, Phys. Rev. Lett. **64**, 3007 (1990).
- [32] H. Matsukawa, J. Phys. Soc. Jpn. **57**, 3463 (1988).
- [33] See *Finite-Size Scaling*, edited by J. L. Cardy (North-Holland, 1988).
- [34] J. Z. Imbrie, Comm. Math. Phys. **98**, 145 (1985).
- [35] S. Coppersmith, Phys. Rev. Lett. **65**, 1044 (1990).
- [36] S. S. Manna, J. Stat. Phys. **59**, 509 (1990). Note that the exponent here of  $\kappa/d$  is analogous to the exponent  $\tau$ .
- [37] Z. Z. Wang and N. P. Ong, Phys. Rev. Lett. **58**, 2375 (1987).
- [38] As in models of non-linear fluid flow in random media; see O. Narayan and D. S. Fisher, preprint.

- [39] For small  $h_0$ , there is no reversible regime in mean field theory; however, there appears to be a pathology at this limit.
- [40] Note that problems with universality in mean field theory arise from the contributions of *both* the jumps and the smooth evolution to quantities such as the dynamic exponent  $\zeta$  above threshold (with CDW velocity  $v \sim f^\zeta$ ). Below four dimensions, the jumps dominate and each region feels a strongly jerky, rather than reasonably smooth, force from the jumps of the other regions. The critical behavior above threshold then becomes universal, see references [3,15].

## TABLES

TABLE I. Numerical results for critical exponents of the charge-density wave model defined by Eq. (1.2).

Exponent	Definition	$d = 1$			$d = 2$		
$\gamma$	Divergence of total polarizability (irreversible path), Eq. (1.7)	3.0	$\pm$	0.5	1.8	$\pm$	0.15
$\rho$	Size dependence of configuration width at threshold, Eq. (4.2)	1.3	$\pm$	0.3	0.8	$\pm$	0.2
$\nu_T$	Size dependence of threshold field distribution, Eq. (5.2)	2.01	$\pm$	0.02	1.01	$\pm$	0.03
$\nu_n$	Finite-size crossover field of polarization, Eq. (5.3)	2.0	$\pm$	0.5	1.0	$\pm$	0.1
$\kappa$	Avalanche size distribution near threshold, Eq. (5.6)	—			0.34	$\pm$	0.10
$\gamma_\ell^R$	Cusp in linear polarizability (reversible path), Eq. (1.9)	—			-0.42	$\pm$	0.05
$\gamma_\ell^I$	Cusp in linear polarizability (irreversible path), Eq. (1.8)	—			-0.40	$\pm$	0.12
$\alpha$	Distribution of linear eigenvalues at threshold, Eq. (4.17)	—			0.84	$\pm$	0.12 <sup>a</sup>
$\nu_\ell$	Finite size crossover of linear polarizability (reversible path), Eq. (1.12)	—			0.44	$\pm$	0.08

<sup>a</sup> Calculated using Eq. (4.19)

## FIGURES

FIG. 1. A schematic illustration in one dimension of the “no-passing” rule for CDW configurations. The lines show the phases,  $\varphi_i$ , as a function of position,  $i$ , for two configurations, one of which (open circles) initially trails (is less than) the other (solid circles) at time  $t = 0$ . Both configurations are driven by the same external field  $F(t)$ . As the configurations evolve from their initial positions, according to the equations of motion Eq. (1.2), they may come close to intersecting, as shown in the figure for  $t > 0$ . They never cross, though: as the two configurations approach each other at some site, the drive and pinning forces on the phase at that site tend to cancel, but the elastic forces, which tend to flatten out the configuration, do not allow the configurations to pass through each other. The arrows indicate the relative elastic forces for  $t > 0$ .

FIG. 2. An illustration of the partial ordering of the configurations in the static state. The lines show the phases  $\varphi_i$  as a function of position in the lattice,  $i$ , for static solutions to the equations of motion for the CDW. The lowest line shows the initial configuration  $\{\varphi_i(0)\}$  static at field  $F(0)$ , while the other lines show configurations  $\{\varphi_i^*\} \in \mathcal{A}^*(\varphi_i(0))$  which is the set of configurations with  $\varphi_i^* \geq \varphi_i(0)$ , for all  $i$ , that are static at the field  $F^*$ , where  $F \leq F^* \leq F_T^+$ . Given the initial configuration  $\{\varphi_i(0)\}$ , if the field is raised to  $F^*$ , the configuration must converge to the unique configuration,  $\{\varphi_i^\infty\}$ , shown as the heavy line, which is the *lowest* stationary configuration that is *above* the initial configuration. The configurations that are static at  $F^*$  and exceed the initial configuration may cross each other as shown, but no configuration in  $\mathcal{A}^*$  may cross the configuration  $\{\varphi_i^\infty\}$ .

FIG. 3. Plot of the polarization,  $P$ , vs. applied field,  $F$ , for a two-dimensional system of size  $64^2$ . The initial configuration is the configuration static at the negative threshold field,  $F_T^-$ . The applied field is increased to the upper threshold value,  $F_T^+$ , and then lowered again. This particular history of applied field, for an adiabatic variation of the field, defines two approaches to threshold: the initial path in configuration space from  $F_T^-$  to  $F_T^+$  is the “irreversible” path and the path for decreasing field, near  $F_T^+$ , defines the “reversible” path.



FIG. 4. The polarization at threshold,  $P_T = P(F_T^+) - P(F_T^-)$ , plotted as a function of the size of the system  $L$  for one and two dimensions. Straight lines showing power law behavior  $P_T \sim L^\rho$  with  $\rho = 1.3 \pm 0.3$  and  $0.8 \pm 0.2$  are shown, corresponding to the estimated exponents for one and two dimensions, respectively.

FIG. 5. Polarization  $P$  vs. reduced field  $f$  for one-dimensional lattice CDW systems, for the irreversible approach to threshold. The sample sizes (and number of realizations averaged over) are indicated. The dashed line shows power law behavior  $P \sim |f|^{-\gamma+1}$  with  $\gamma = 3.0 \pm 0.5$ .

FIG. 6. Polarization  $P$  vs. reduced field  $f$  for the irreversible approach to threshold in two dimensions. The system sizes (number of realizations) are indicated. The straight line shows power law behavior,  $P \sim |f|^{-\gamma+1}$ , with  $\gamma = 1.8 \pm 0.15$  determined by the fits to the polarizability shown in Fig. 7.

FIG. 7. Polarizability  $\chi^\uparrow(f)$  for the irreversible path in two dimensions, which is found by calculating the numerical derivative of the data of Fig. 6, i.e., the difference of the polarization between two consecutive data points. The straight line shows a fit to the form  $\chi^\uparrow \sim |f|^{-\gamma}$ , with  $\gamma = 1.8 \pm 0.15$ .

FIG. 8. The polarization  $P$  as a function of the magnitude of the reduced field  $|f|$  on a irreversible approach to threshold (see text), for single samples in  $d = 3$  of size  $64^3$  and  $128^3$ . The critical behavior is difficult to determine with confidence, but note that the polarization exceeds  $2\pi$  only for fields within 0.1% of threshold. The dotted line shows an exponent  $\gamma = 0.33$  for comparison only.

FIG. 9. A fine scale plot of the polarization  $P$  (upper curve, right scale) and linear polarizability  $\chi_0$  (lower curve, left scale) for the irreversible path (increasing  $F$ ) for a single system of size  $128^2$ . The discontinuities in the polarization are due to the jumps that occur when a local minimum of the potential vanishes. The corresponding spikes in  $\chi_0$  are due to the diverging linear response as these jumps are approached (the divergence has been cut off at an arbitrary value for the plot). From the size of the jumps in the polarization, it can be seen that, for reduced fields of this order, the jumps involve only a few of the degrees of freedom. In an infinite system, the jumps occur at a dense set of fields, but the fraction of the field range in which the linear polarizability is affected by the divergences goes to zero as the system size approaches infinity. The dotted line indicates an envelope function, which, in the infinite volume limit, gives  $\chi_0(F)$  with probability one.

FIG. 10. Plot of the derivative of the linear polarizability,  $d\chi_0(f)/dF$ , vs. reduced field  $f$  for two-dimensional systems of various sizes, for the reversible approach to threshold. The fit indicated by the slope of the dashed line gives  $d\chi_0(f)/dF \sim f^{-\gamma_\ell^R-1}$  with  $\gamma_\ell^R = -0.42 \pm 0.05$ .

FIG. 11. Plot of  $\chi_T - \chi_0(f)$  for reversible (open symbols) and irreversible (closed symbols) approaches to threshold in two dimensions. The threshold polarizability  $\chi_T$  is calculated from the data for  $d\chi_0/dF$  along the reversible path. Straight lines show fits to cusp-like behavior  $\chi_0(f) \simeq \chi_T - A^{(R,I)} f^{-\gamma_\ell^{(R,I)}}$ , where the reversible path exponent,  $\gamma_\ell^R$ , is found to be  $-0.42 \pm 0.05$  and the irreversible path exponent  $\gamma_\ell^I = -0.40 \pm 0.12$ . Error bars indicate statistical uncertainties for the reversible path and the uncertainty in  $\chi_T$  for data on the irreversible path; statistical errors for the irreversible path are of the order of the fluctuations about the fit.

FIG. 12. Plot of the square of the linear eigenvalues,  $\Lambda_m^2$ , vs. reduced field  $f$  for the lowest eigenmodes  $m = 0, 1, 2$ , in  $d = 2$  on the reversible approach to threshold. The straight lines show fits  $\Lambda_m^2 \sim (f_m^c - f)$ . The extrapolations shown for  $f > 0$ , which determine  $f_m^c$ , are not physical, as once the lowest mode becomes unstable ( $\Lambda_0 = 0$ ), the CDW is in the sliding state.

FIG. 13. Scaling picture of the density of states  $\rho(\Lambda)$ . The dashed line shows the density of states for the threshold configuration, which behaves as a power law  $\rho \sim |\Lambda|^\alpha$  for small  $\Lambda$ . The upper curve, diverging at finite  $\Lambda$  and vanishing for smaller  $\Lambda$ , gives the density of states for the reversible path, while the lower curve, linear at the origin, shows the density of states for the irreversible path. Though the distributions for the two histories differ in shape, they share a common scaling form,  $\rho(\Lambda) \sim \Lambda^\alpha \hat{\rho}(\Lambda/f^\mu)$ , with the characteristic scale  $f^\mu$  (indicated by the vertical dotted line) the same for both histories.

FIG. 14. Average threshold field,  $F_T$ , as a function of linear size,  $L$ , in one and two dimensions. The error bars show the statistical error in the average of the threshold field; the width of the distribution of threshold fields at each size is larger (see Fig. 16.)

FIG. 15. Distribution of threshold fields calculated for 128 samples of linear size  $L = 32$  in two dimensions (solid line). For comparison, a Gaussian fit is shown (dotted line).

FIG. 16. A plot of the width of the threshold-field distribution,  $\Delta F_T(L)$ , vs. linear size,  $L$ , in one and two dimensions. Lines show least square fits to the data for  $L \geq 16$ . From the slopes of these lines, we find values for the finite-size-scaling exponent  $\nu_T$  of  $2.01 \pm 0.02$  and  $1.01 \pm 0.03$  in one and two dimensions, respectively.

FIG. 17. Scaling plot of  $P|f|^{\gamma-1}$  vs.  $L|f|^{\nu_n}$  for the polarization of two-dimensional systems, for best fit values of  $\nu_n = 1.0 \pm 0.1$  and  $\gamma = 1.8 \pm 0.1$ . The deviations apparent at large  $L|f|^{\nu_n}$  occur for large reduced fields  $1.0 > |f| > 0.2$ , where corrections to scaling are pronounced.

FIG. 18. Plot of  $P|f|^\gamma$  vs.  $L|f|^{\nu_n}$  for the one-dimensional lattice CDW model, with exponents  $\nu_n = 2.0$  and  $\gamma = 3.5$ . No choice for these exponents gives a single curve which fits all of the data.

FIG. 19. Individual avalanche events, indicated by avalanche size  $\Delta P$  on a logarithmic scale and the field  $F$  at which the avalanche occurs, for a system of size  $256^2$  on the path  $\{\varphi_i^\dagger F\}$ ; each point corresponds to a single event. The solid line indicates a size dependence  $\sim (F_T^+ - F)^{-d\nu}$ , with  $\nu = 1.0$ . The region outlined by the dashed line indicates the events used to determine the near-critical avalanche size distribution in Fig. 20.

FIG. 20. Logarithmically binned distribution  $N(\Delta P)$  of avalanche sizes  $\Delta P$  for the events in the near-critical region indicated by the dashed line in Fig. 19. The solid line shows the fit  $N(\Delta P) \sim \Delta P^{-\kappa/d}$ , for  $\kappa = 0.34 \pm 0.10$ .

FIG. 21. Scaled plot of  $d\chi_0(f)/dF$  for the reversible path in two-dimensional systems, using the best-fit finite-size scaling exponent  $\nu_\ell = 0.44$ . Representative error bars show the statistical uncertainty in the scaled  $d\chi_0(f)/dF$ ; for  $|f|L^{1/\nu_\ell} > 100$ , the error bars are smaller than the symbol size.

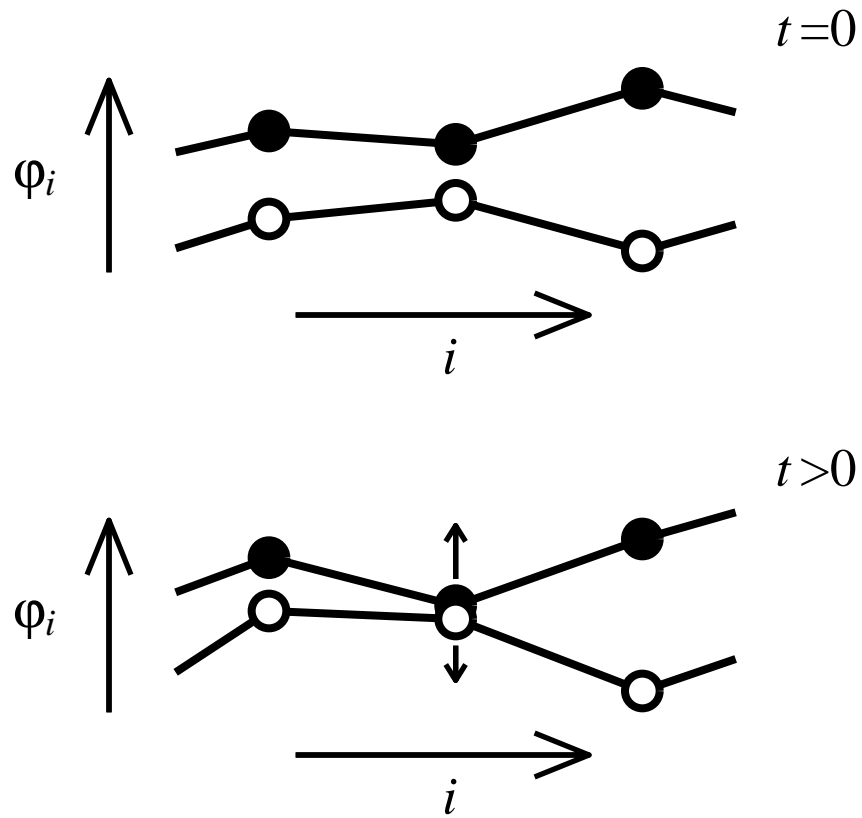


Fig. 1 - Fisher and Middleton, "Critical Behavior of Charge Density ..."

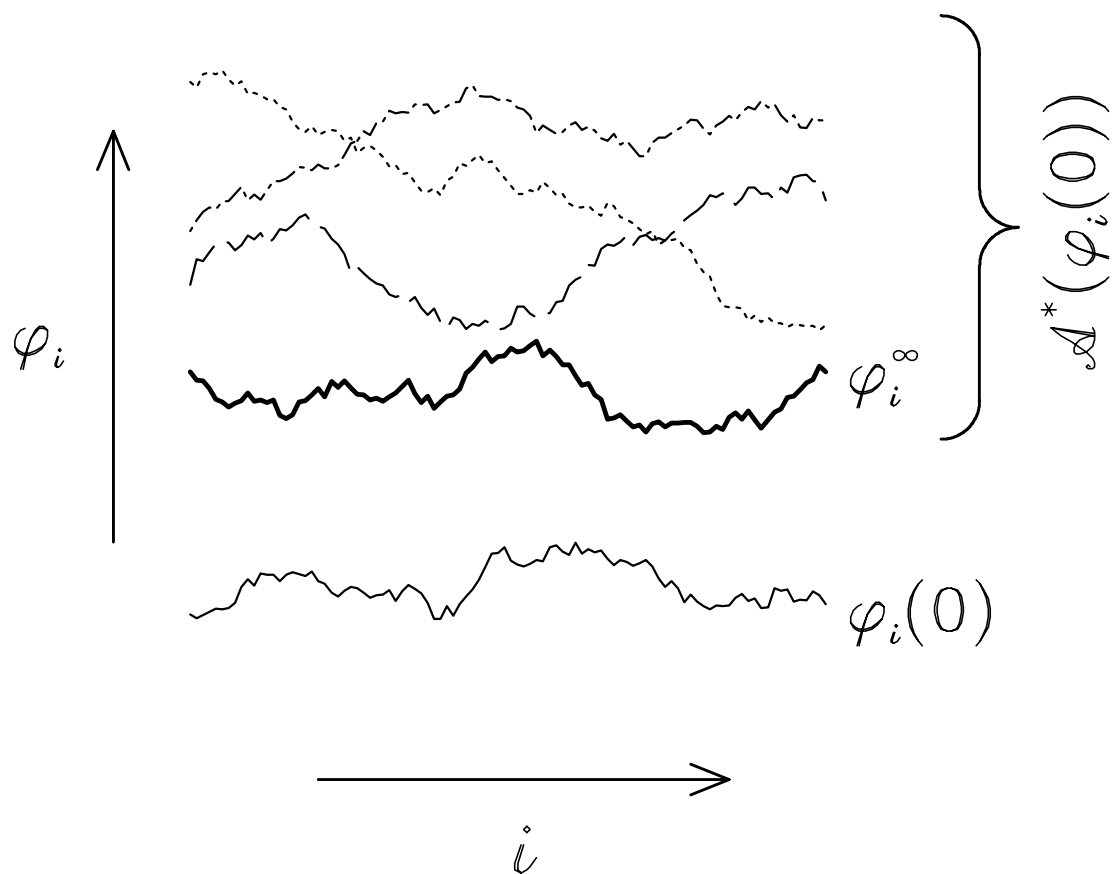


Fig. 2 - Fisher and Middleton, "Critical Behavior of Charge Density ..."

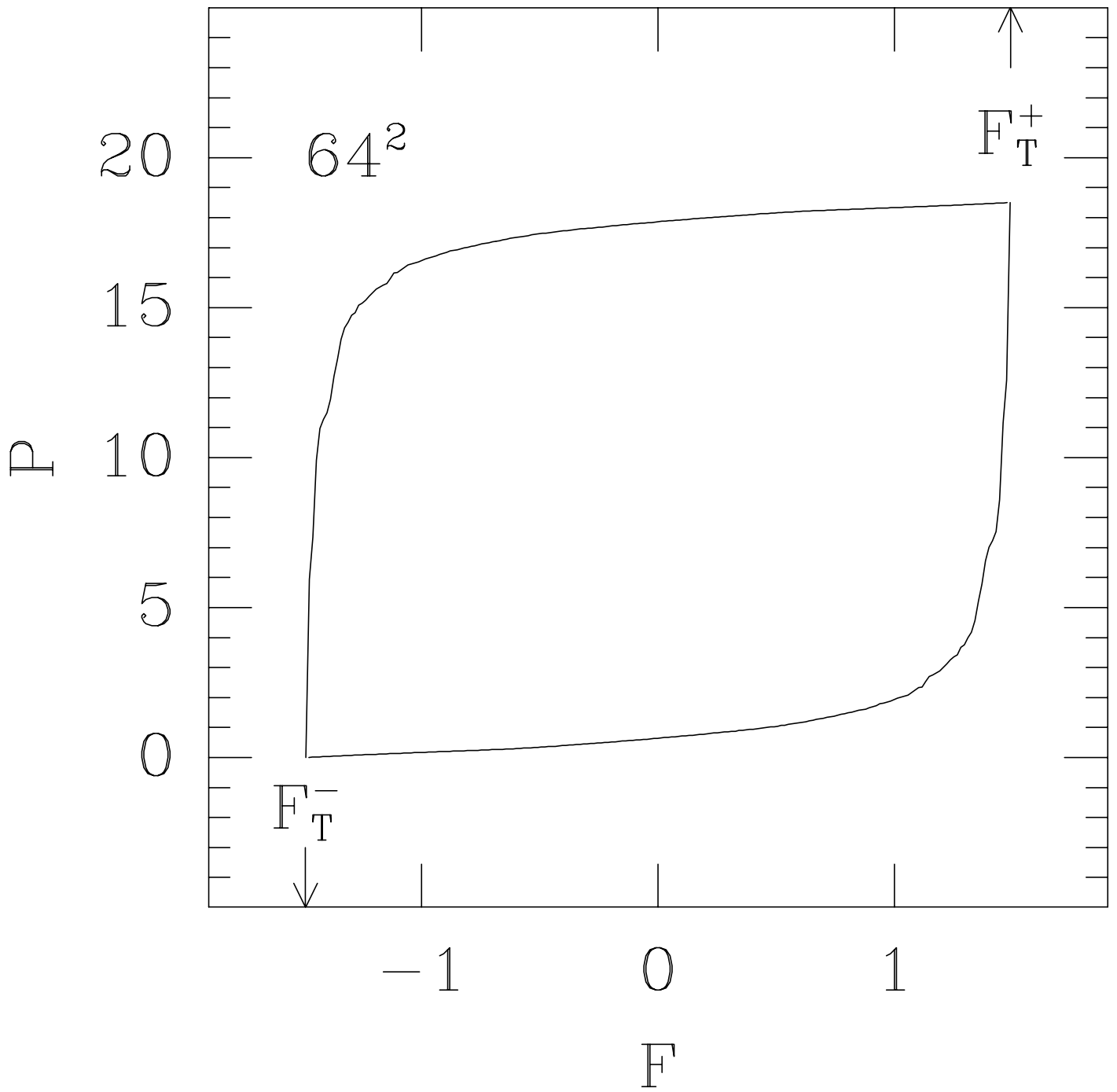


Fig. 3 - Fisher and Middleton, "Critical Behavior of Charge Density ..."

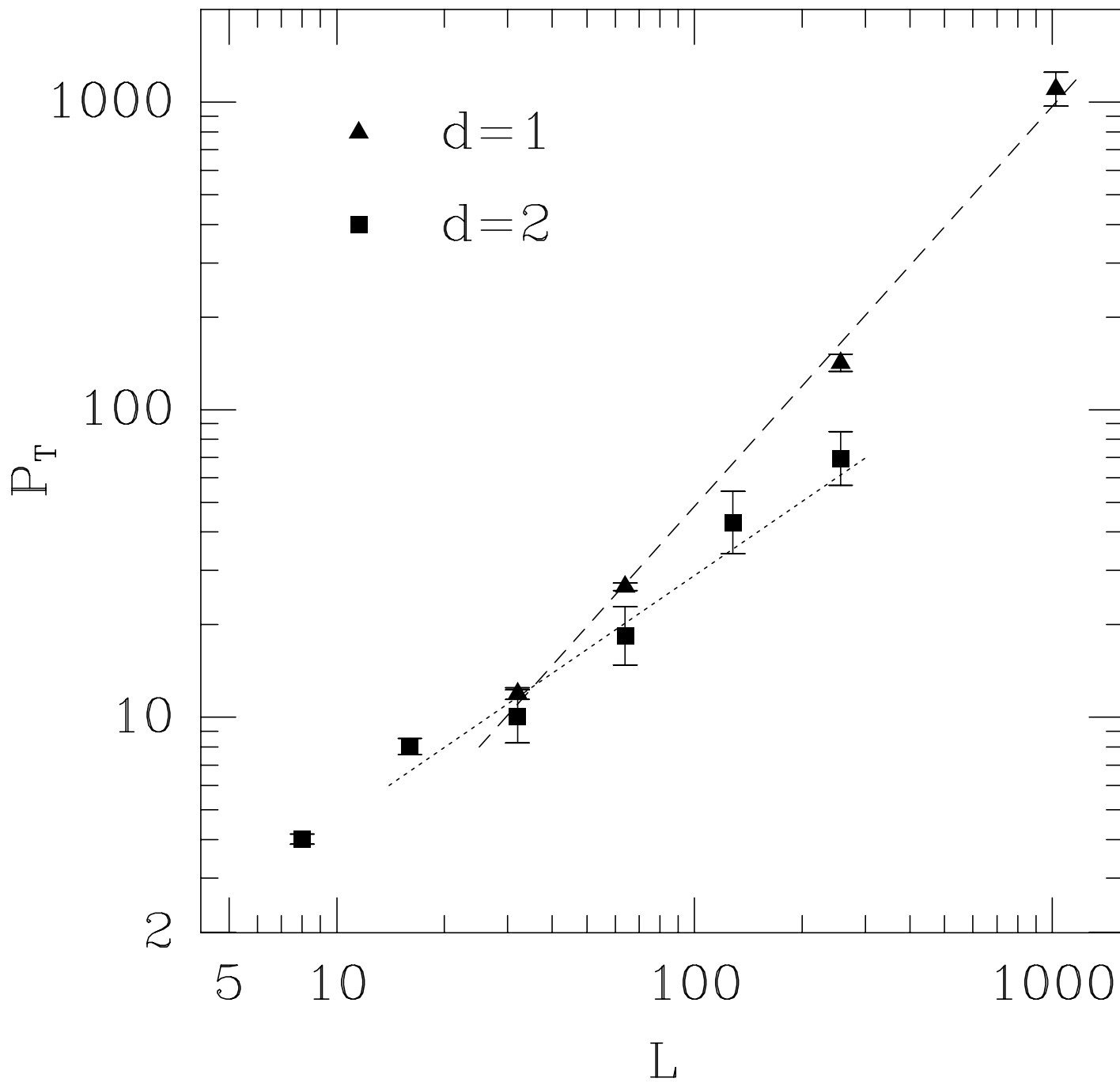


Fig. 4 - Fisher and Middleton, "Critical Behavior of Charge Density ..."



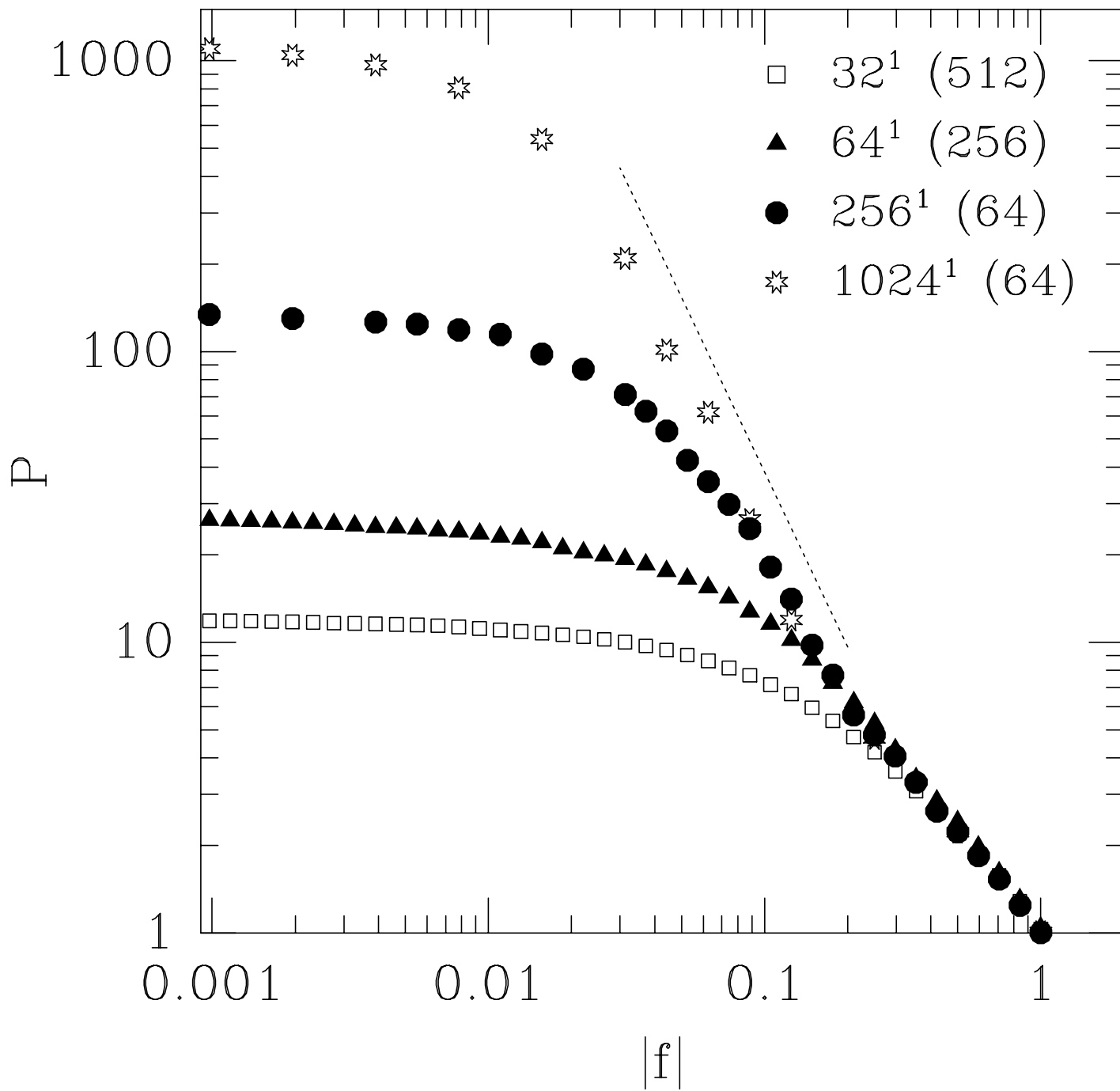


Fig. 5 - Fisher and Middleton, "Critical Behavior of Charge Density ..."

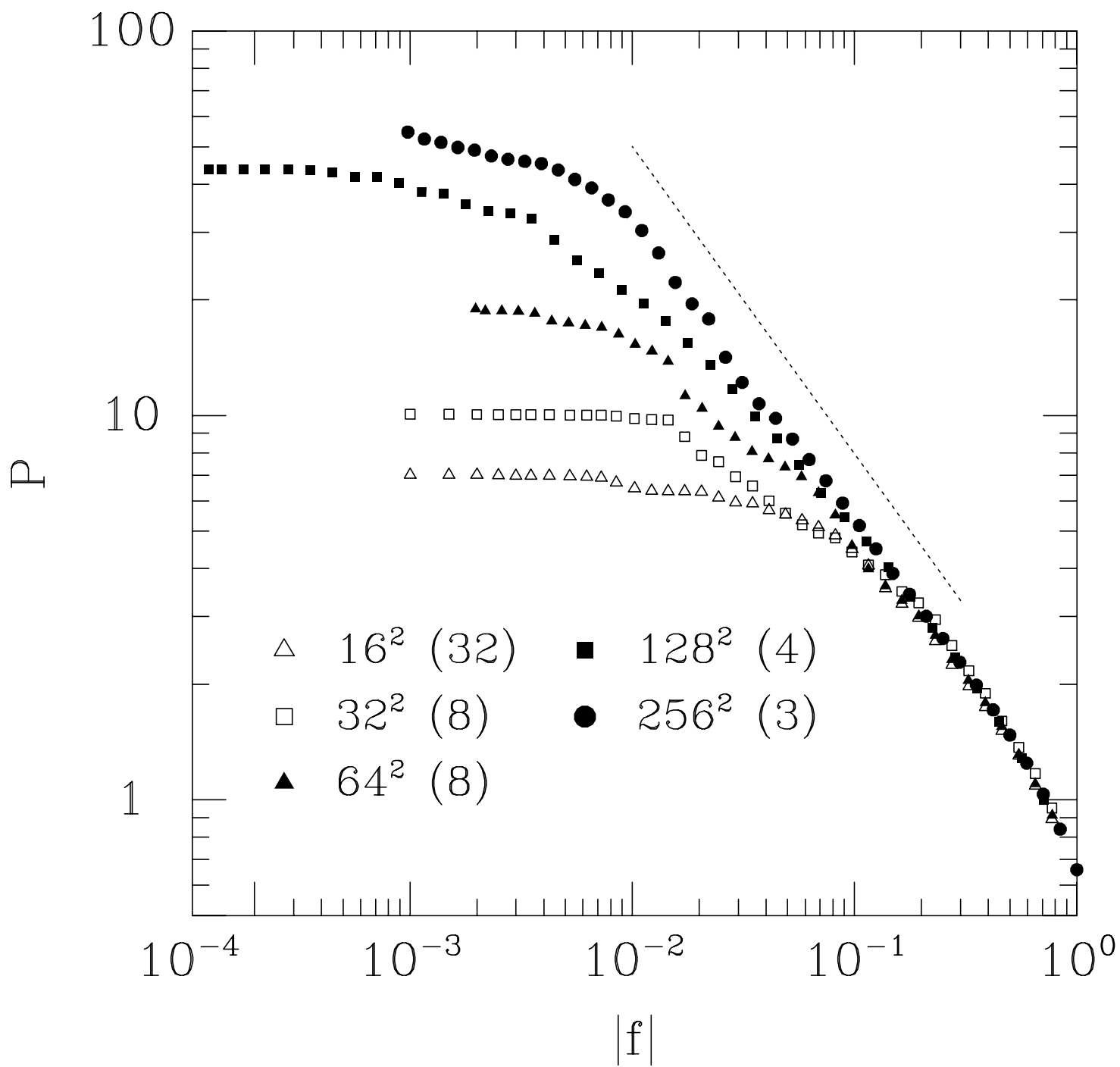


Fig. 6 - Fisher and Middleton, "Critical Behavior of Charge Density ..."

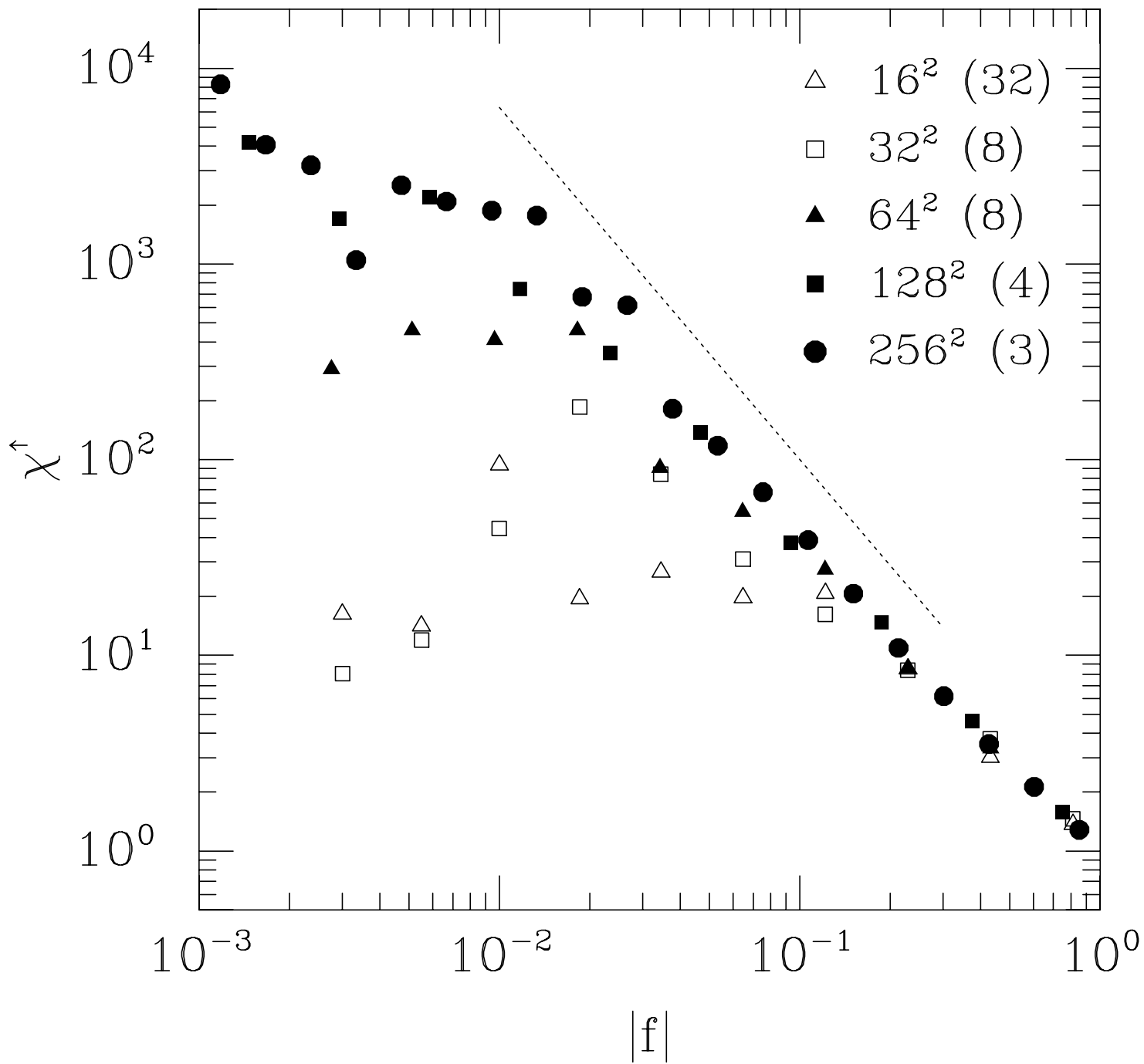


Fig. 7 - Fisher and Middleton, "Critical Behavior of Charge Density ..."

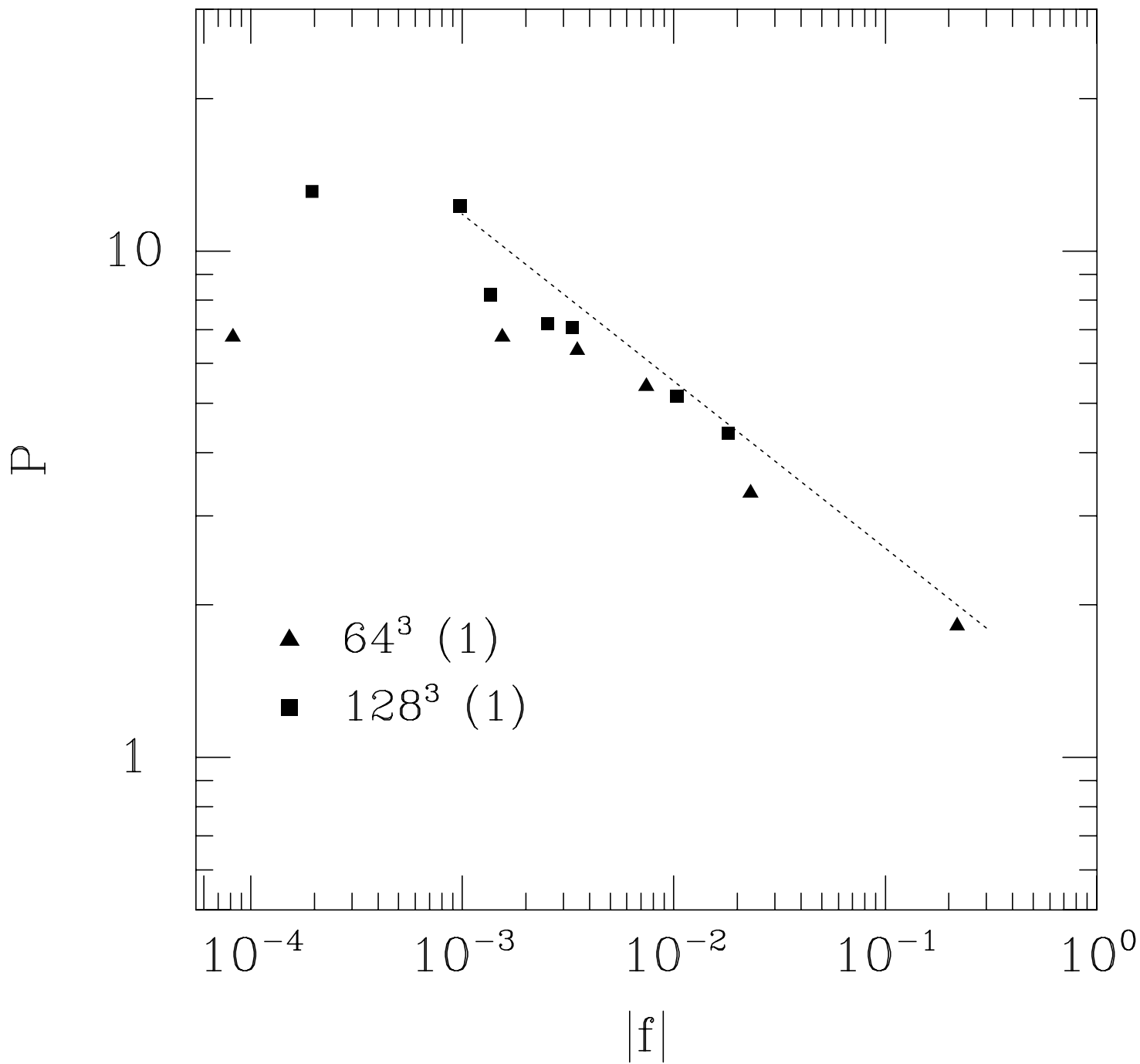


Fig. 8 - Fisher and Middleton, "Critical Behavior of Charge Density ..."

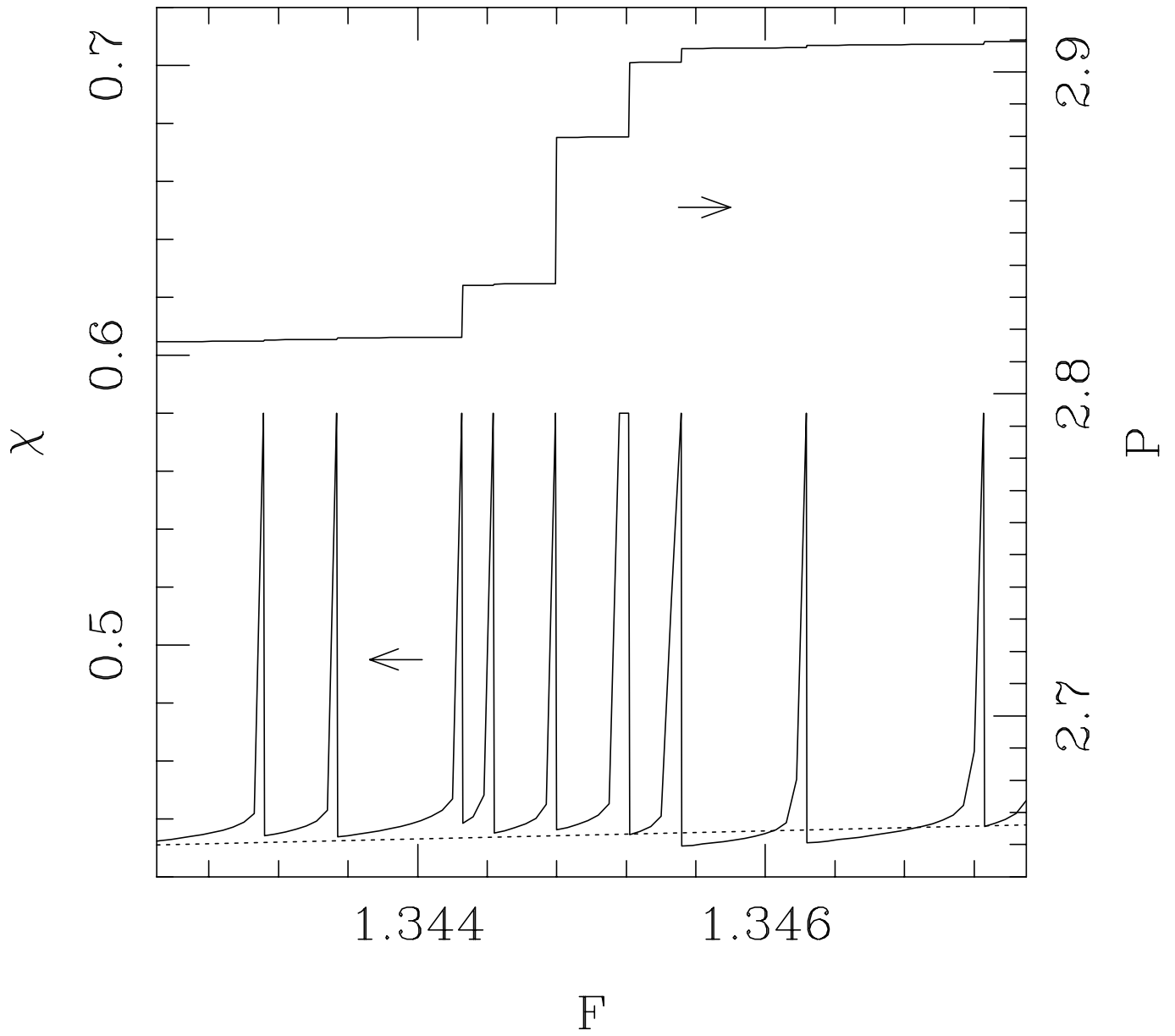


Fig. 9 - Fisher and Middleton, "Critical Behavior of Charge Density ..."

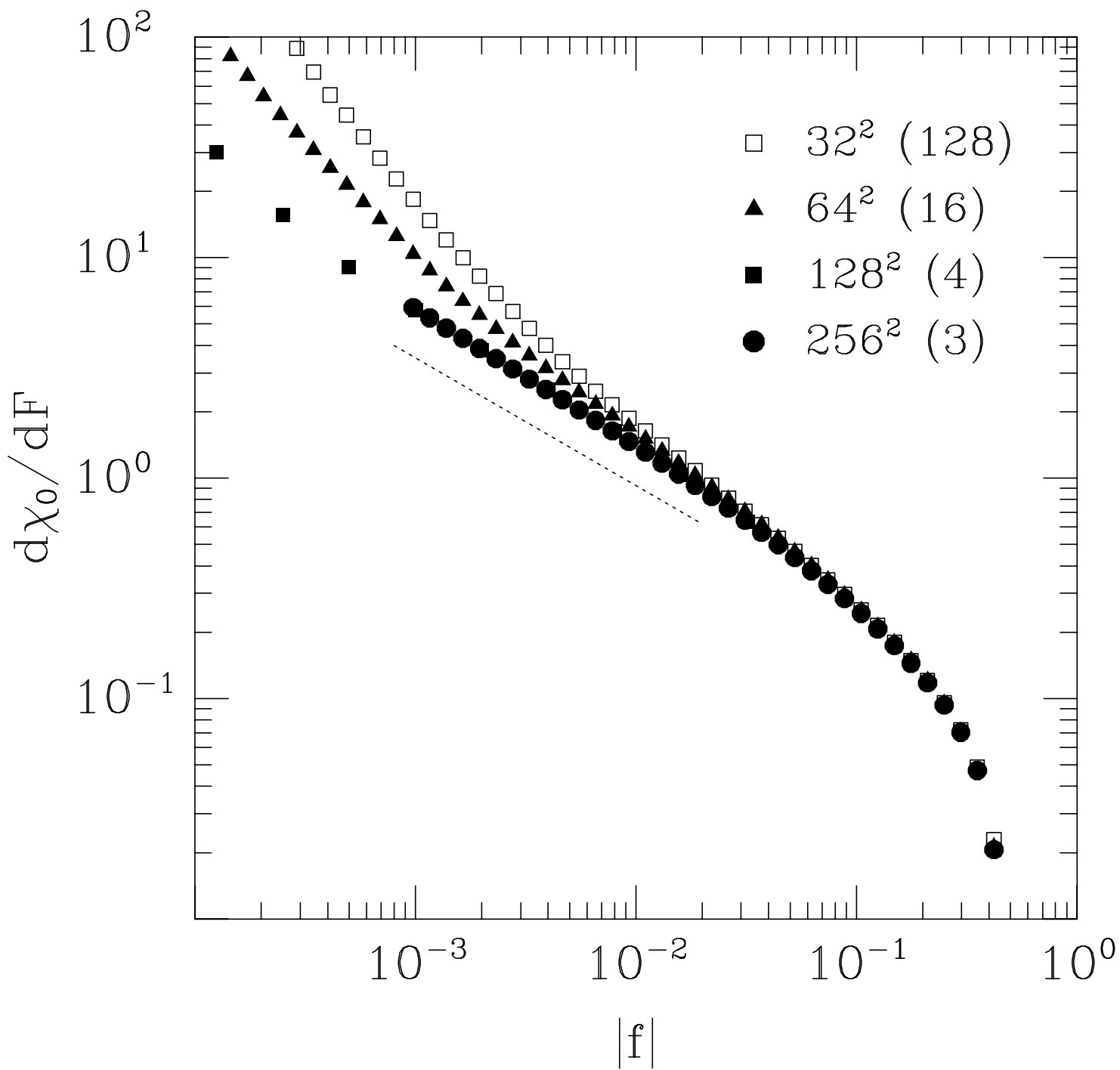


Fig. 10 - Fisher and Middleton, "Critical Behavior of Charge Density ..."

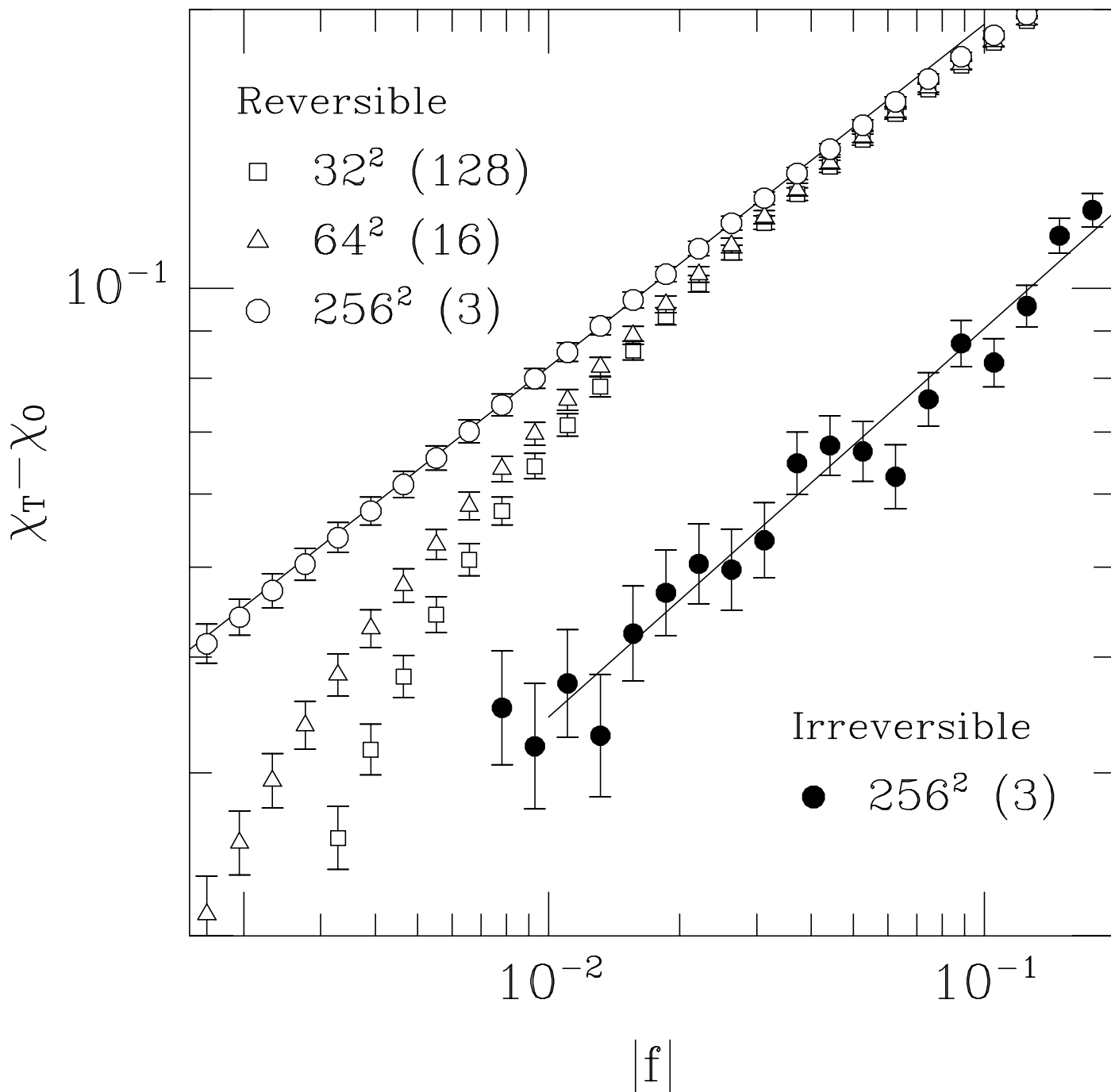


Fig. 11 - Fisher and Middleton, "Critical Behavior of Charge Density ..."

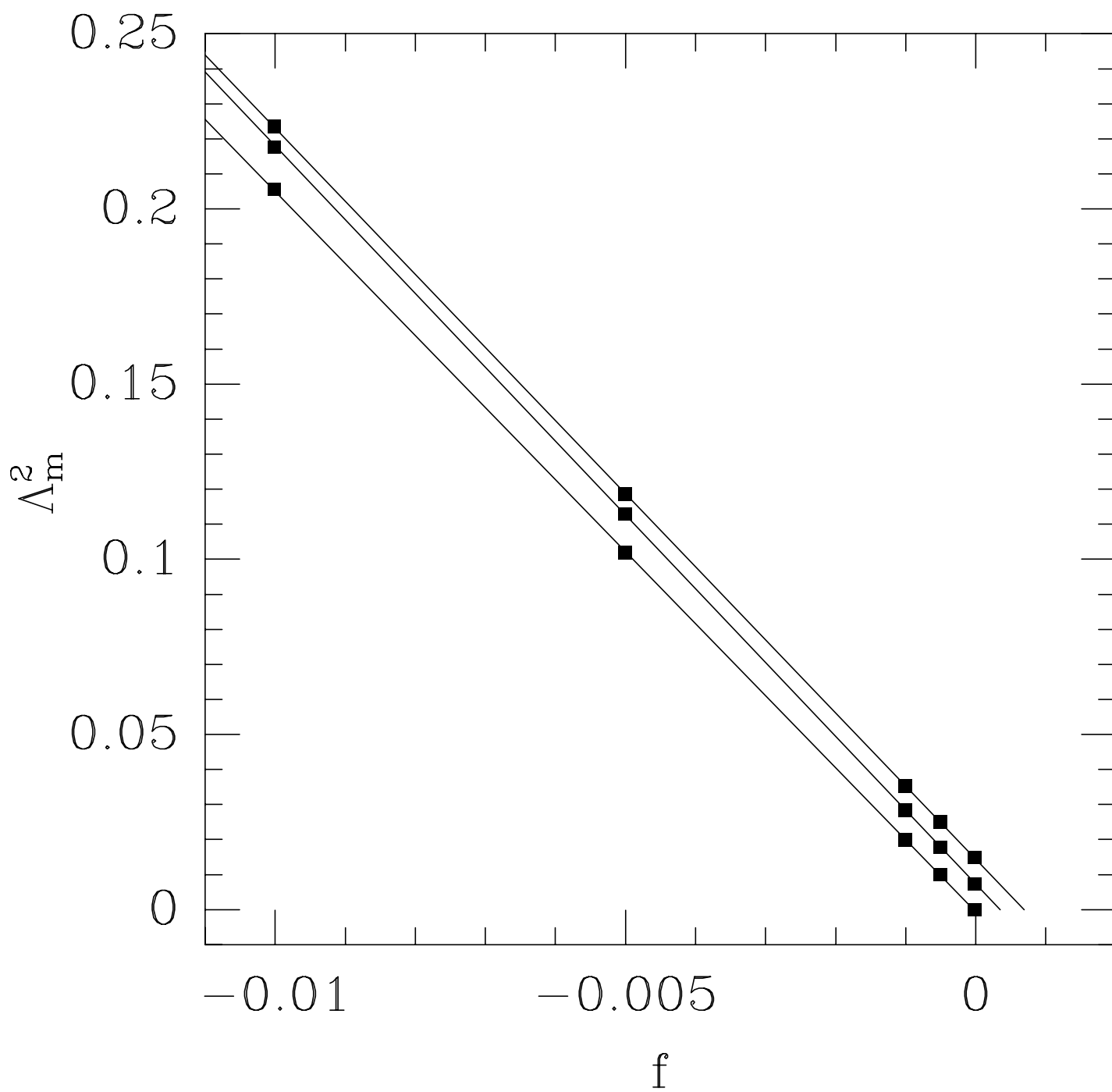


Fig. 12 - Fisher and Middleton, "Critical Behavior of Charge Density ..."



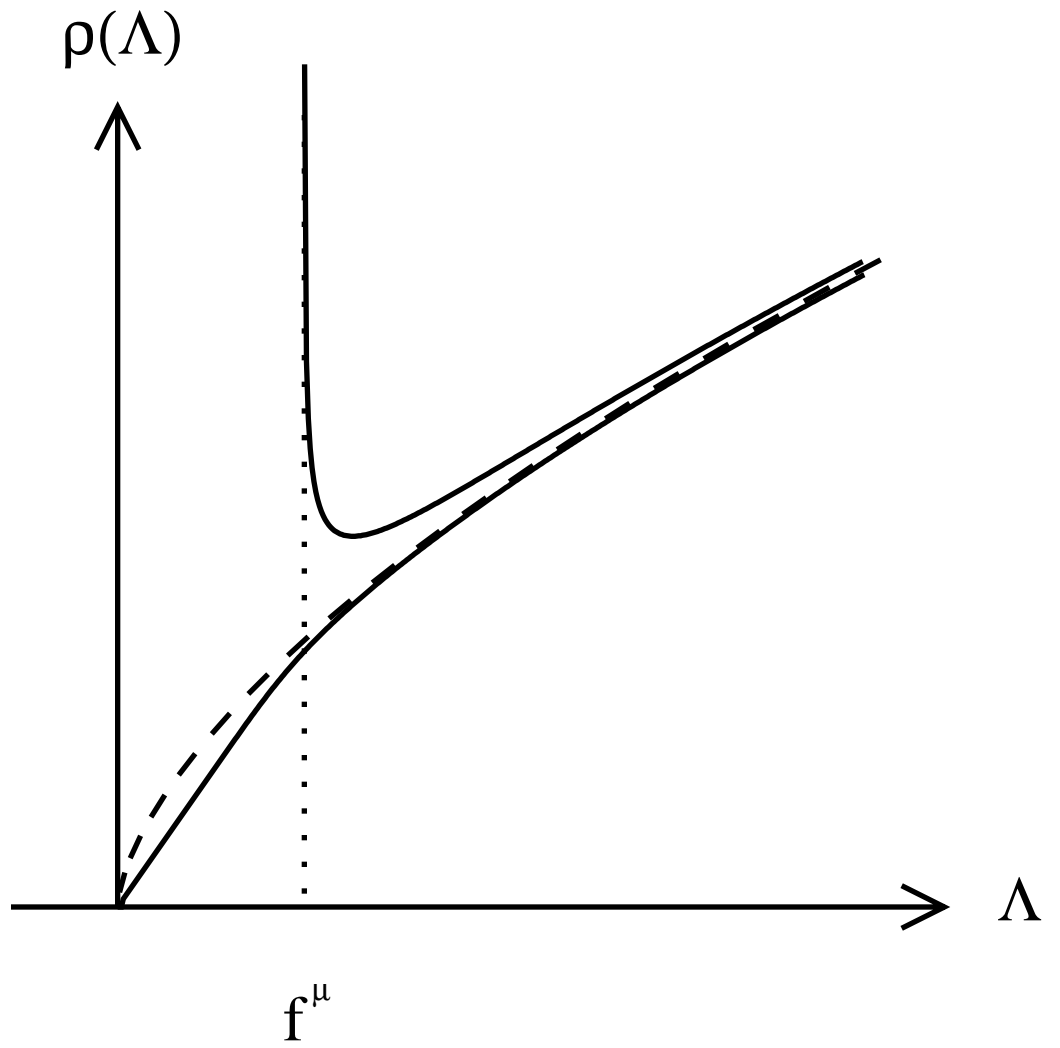


Fig. 13 - Fisher and Middleton, "Critical Behavior of Charge Density ..."

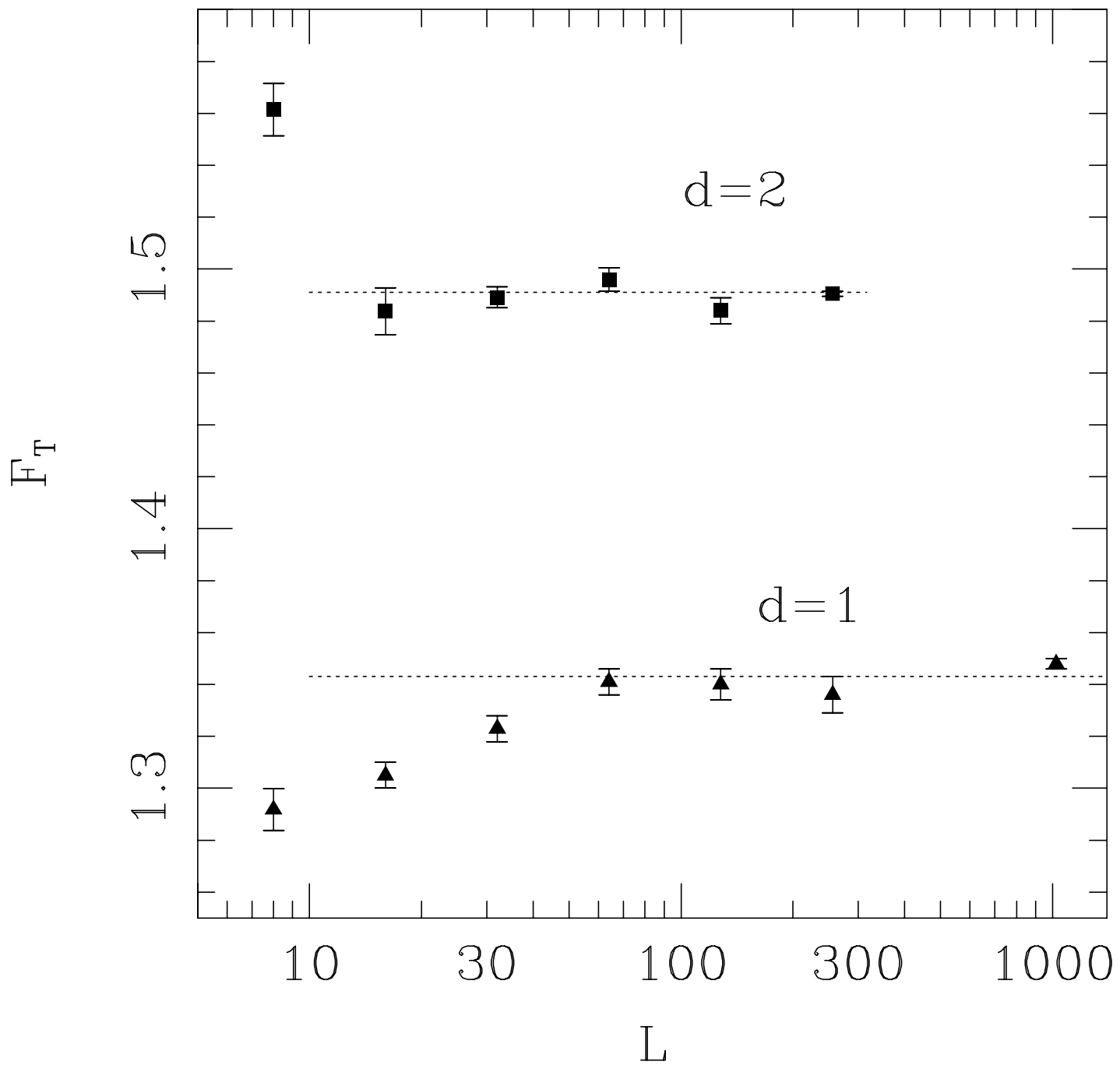


Fig. 14 - Fisher and Middleton, "Critical Behavior of Charge Density ..."

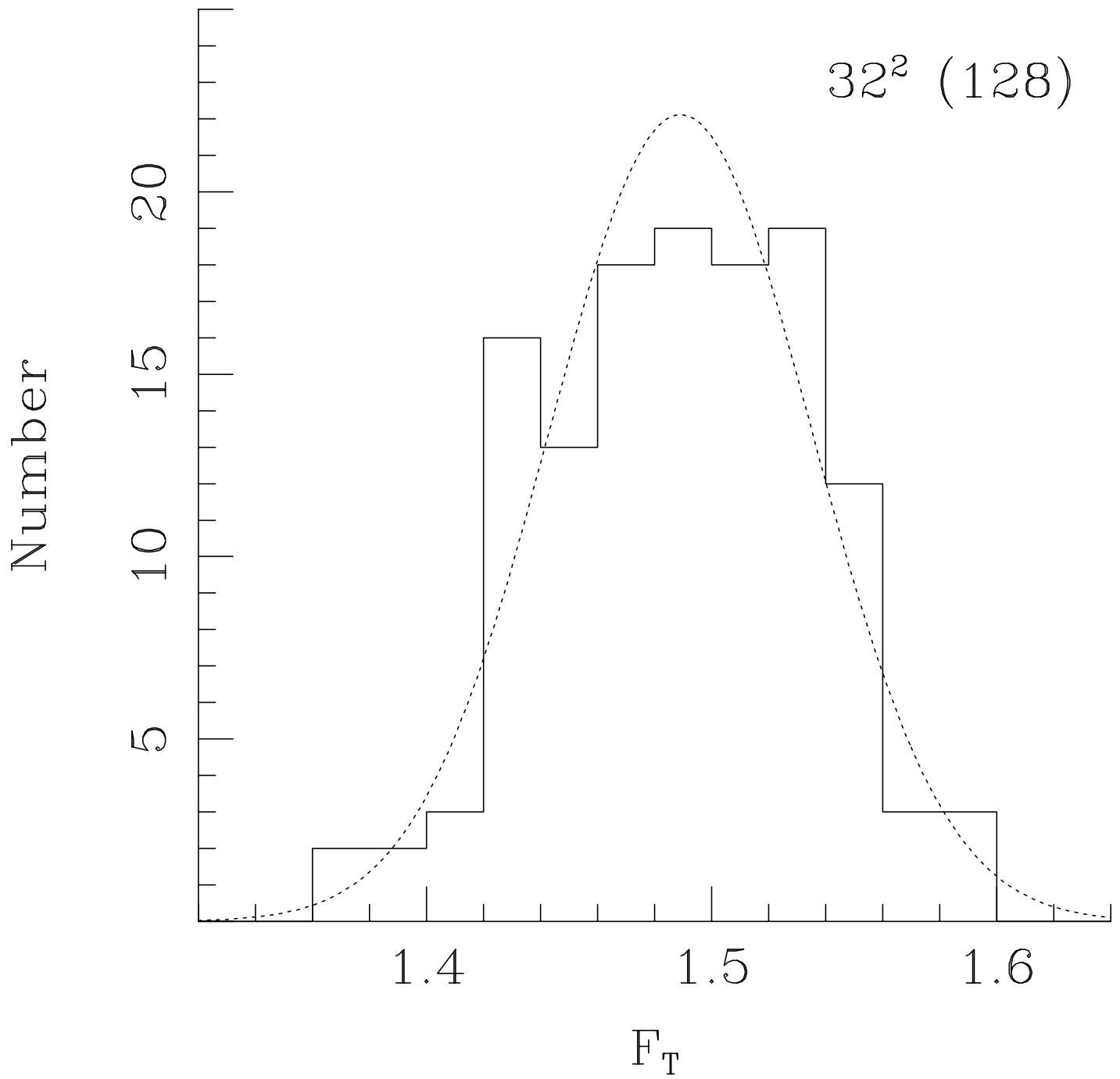


Fig. 15 - Fisher and Middleton, "Critical Behavior of Charge Density ..."

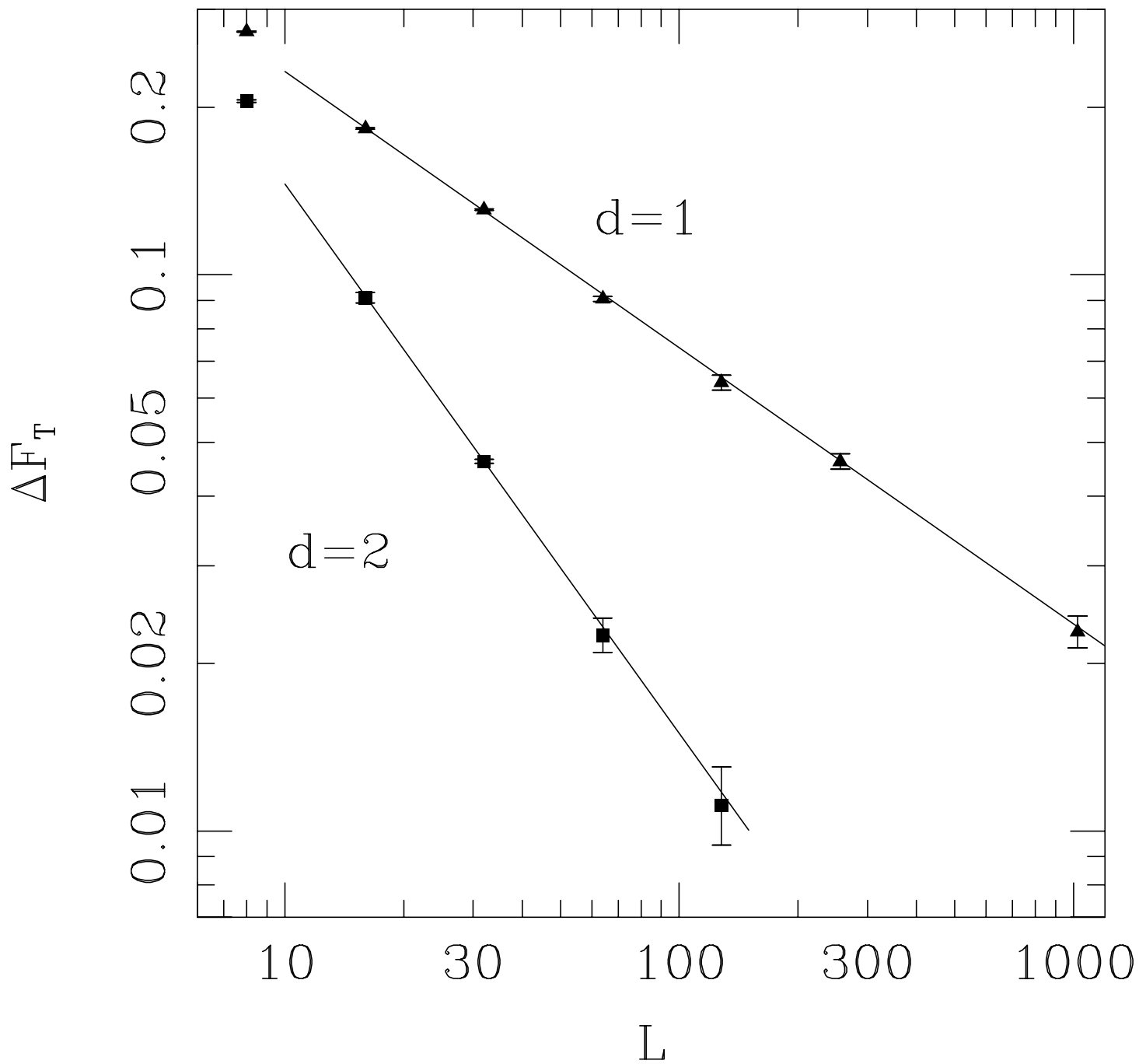


Fig. 16 - Fisher and Middleton, "Critical Behavior of Charge Density ..."

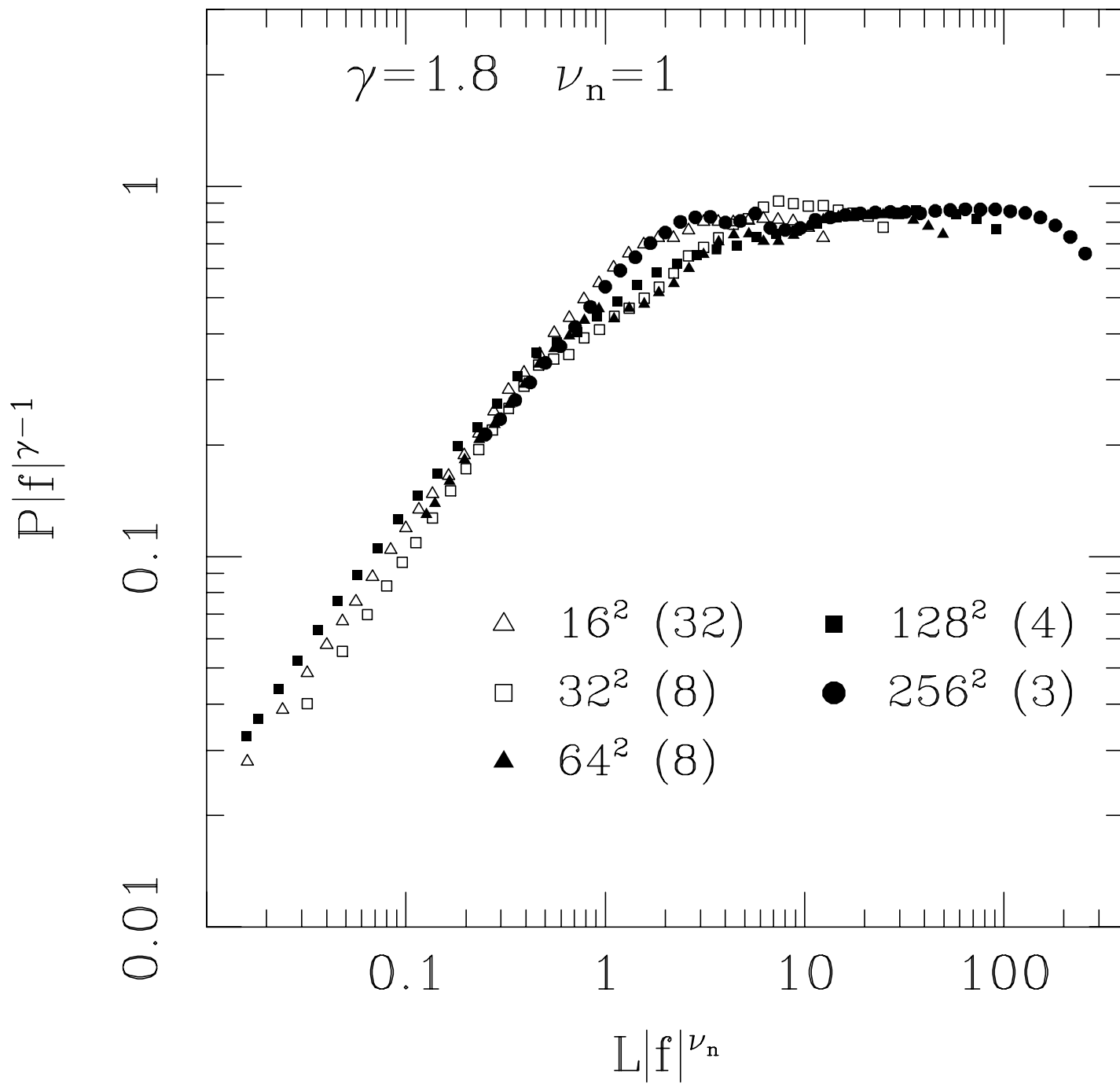


Fig. 17 - Fisher and Middleton, "Critical Behavior of Charge Density ..."

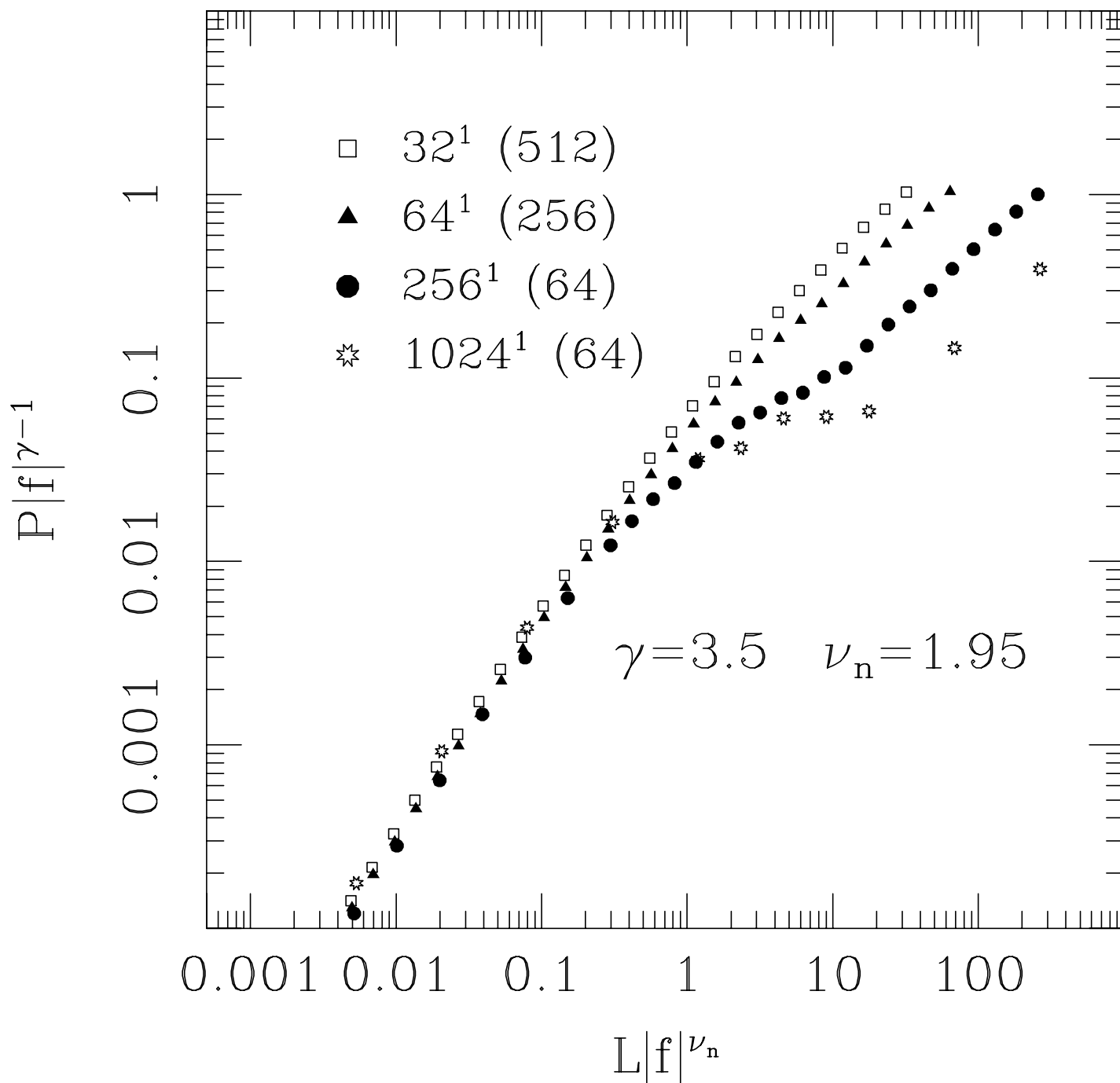


Fig. 18 - Fisher and Middleton, "Critical Behavior of Charge Density ..."

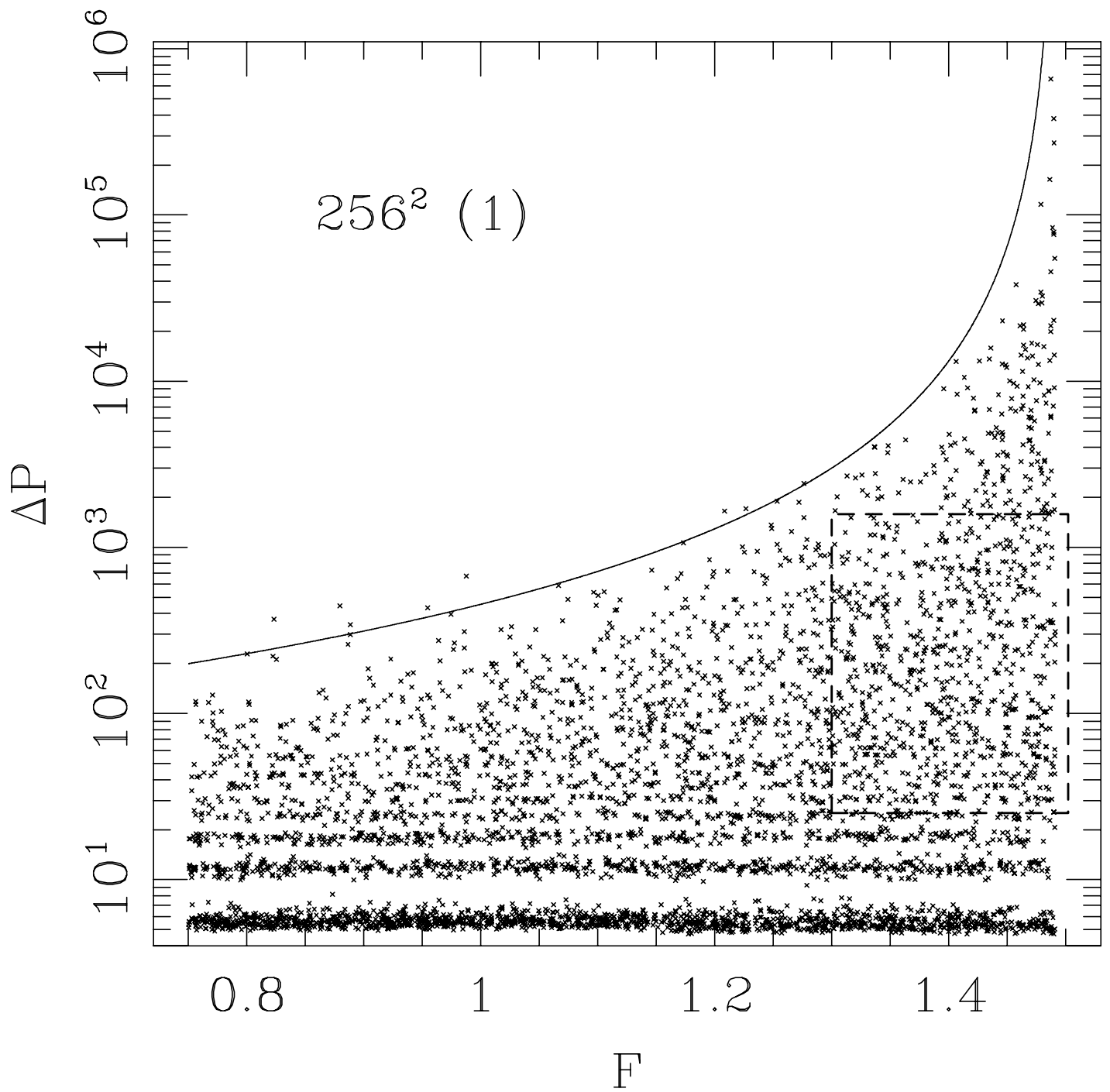


Fig. 19 - Fisher and Middleton, "Critical Behavior of Charge Density ..."

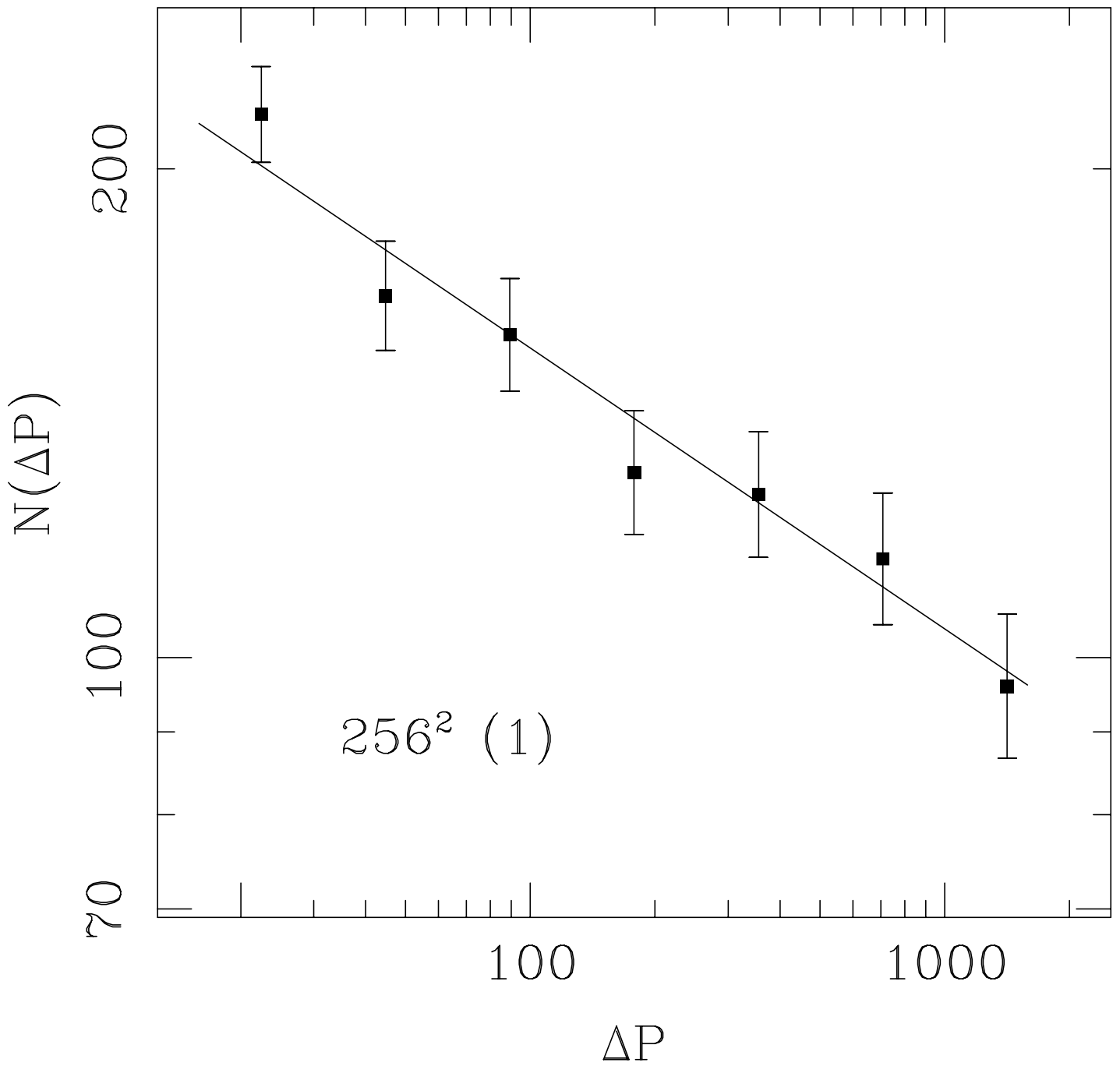


Fig. 20 - Fisher and Middleton, "Critical Behavior of Charge Density ..."



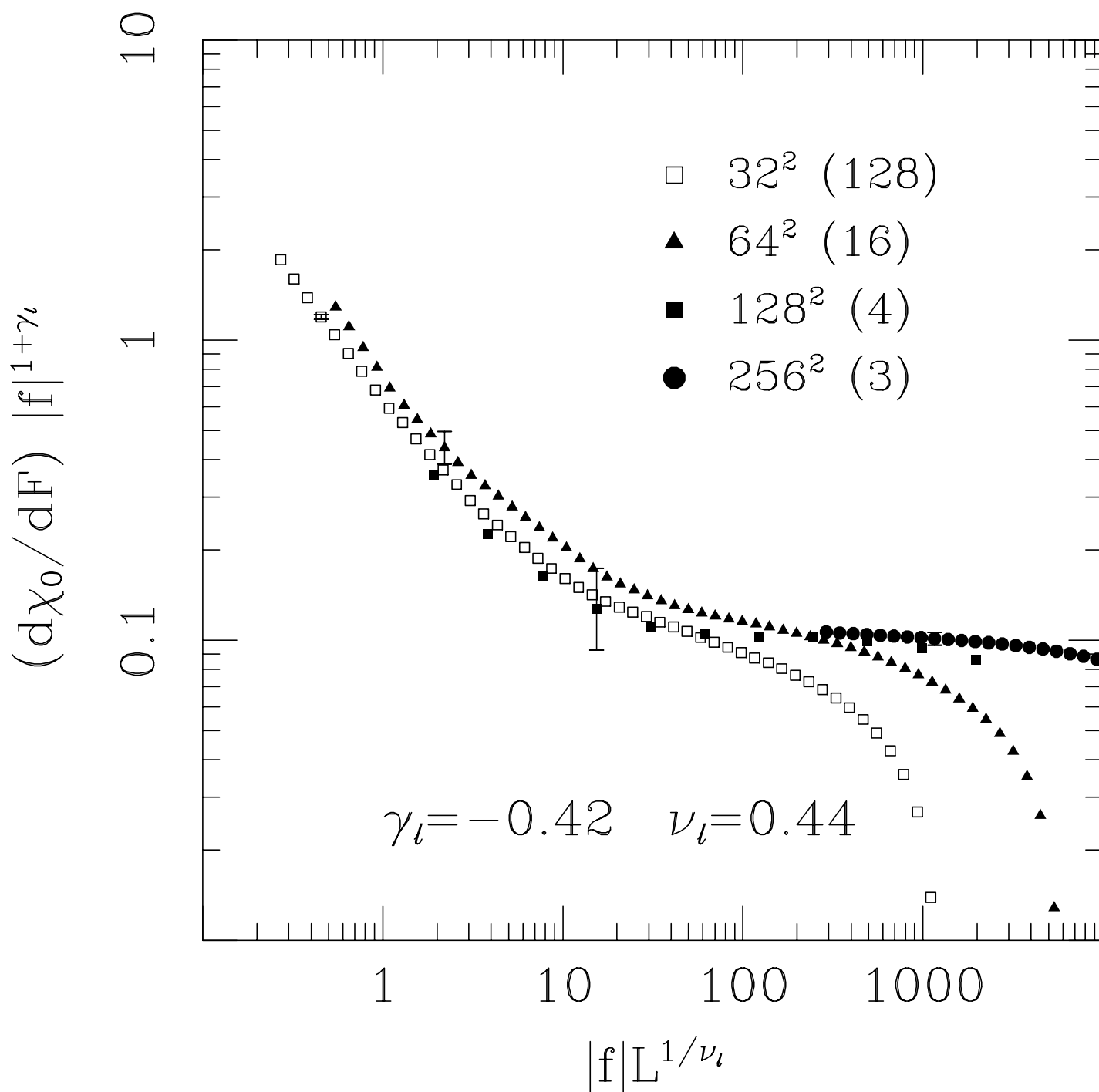


Fig. 21 - Fisher and Middleton, "Critical Behavior of Charge Density ..."